



HAL
open science

Trabecular and cortical bone structure of the talus and distal tibia inPanandHomo

Zewdi J Tsegai, Matthew M Skinner, Andrew H Gee, Dieter H Pahr, Graham M Treece, Jean-Jacques Hublin

► **To cite this version:**

Zewdi J Tsegai, Matthew M Skinner, Andrew H Gee, Dieter H Pahr, Graham M Treece, et al.. Trabecular and cortical bone structure of the talus and distal tibia inPanandHomo. American Journal of Physical Anthropology, 2017, 163, pp.784 - 805. 10.1002/ajpa.23249 . hal-04045434

HAL Id: hal-04045434


<https://hal.science/hal-04045434v1>

Submitted on 24 Mar 2023

HAL is a multi-disciplinary open access archive for the deposit and dissemination of scientific research documents, whether they are published or not. The documents may come from teaching and research institutions in France or abroad, or from public or private research centers.

L'archive ouverte pluridisciplinaire **HAL**, est destinée au dépôt et à la diffusion de documents scientifiques de niveau recherche, publiés ou non, émanant des établissements d'enseignement et de recherche français ou étrangers, des laboratoires publics ou privés.

Trabecular and cortical bone structure of the talus and distal tibia in *Pan* and *Homo*

Zewdi J. Tsegai¹  | Matthew M. Skinner^{1,2} | Andrew H. Gee³ | Dieter H. Pahr⁴ |
Graham M. Treece³ | Jean-Jacques Hublin¹ | Tracy L. Kivell^{1,2}

¹Department of Human Evolution, Max Planck Institute for Evolutionary Anthropology, Leipzig, Germany

²Skeletal Biology Research Centre, School of Anthropology and Conservation, University of Kent, Canterbury, United Kingdom

³Department of Engineering, University of Cambridge, Cambridge, United Kingdom

⁴Institute for Lightweight Design and Structural Biomechanics, Vienna University of Technology, Wien, Austria

Correspondence

Zewdi J. Tsegai, Department of Human Evolution, Max Planck Institute for Evolutionary Anthropology, Deutscher Platz 6, D-04103 Leipzig, Germany.
Email: zewdi_tsegai@eva.mpg.de

Funding information

The Max Planck Society and European Research Council, Grant Number: 336301

Abstract

Objectives: Internal bone structure, both cortical and trabecular bone, remodels in response to loading and may provide important information regarding behavior. The foot is well suited to analysis of internal bone structure because it experiences the initial substrate reaction forces, due to its proximity to the substrate. Moreover, as humans and apes differ in loading of the foot, this region is relevant to questions concerning arboreal locomotion and bipedality in the hominoid fossil record.

Materials and methods: We apply a whole-bone/epiphysis approach to analyze trabecular and cortical bone in the distal tibia and talus of *Pan troglodytes* and *Homo sapiens*. We quantify bone volume fraction (BV/TV), degree of anisotropy (DA), trabecular thickness (Tb.Th), bone surface to volume ratio (BS/BV), and cortical thickness and investigate the distribution of BV/TV and cortical thickness throughout the bone/epiphysis.

Results: We find that *Pan* has a greater BV/TV, a lower BS/BV and thicker cortices than *Homo* in both the talus and distal tibia. The trabecular structure of the talus is more divergent than the tibia, having thicker, less uniformly aligned trabeculae in *Pan* compared to *Homo*. Differences in dorsiflexion at the talocrural joint and in degree of mobility at the talonavicular joint are reflected in the distribution of cortical and trabecular bone.

Discussion: Overall, quantified trabecular parameters represent overall differences in bone strength between the two species, however, DA may be directly related to joint loading. Cortical and trabecular bone distributions correlate with habitual joint positions adopted by each species, and thus have potential for interpreting joint position in fossil hominoids.

KEYWORDS

bipedalism, bone microstructure, cancellous bone, functional morphology, locomotion

1 | INTRODUCTION

Aspects of the external bony morphology of the talus and distal tibia reflect kinematic differences between how terrestrial bipedal humans and arboreal, quadrupedal African apes load their foot and ankle during locomotion (e.g., Barak, Lieberman, Raichlen et al., 2013; DeSilva, 2009; Latimer, Ohman, & Lovejoy, 1987; Lewis, 1980a,b,c; Stern & Susman, 1983). These morphological differences can be related to fundamental differences in foot posture: the degree of dorsiflexion at the ankle, use of the foot in an inverted position, the general conformation of the leg,

and the presence of medial and longitudinal arches of the foot. For example, compared with African apes, humans have been described as having a less mediolaterally expanded anterior distal articular surface of the tibia (DeSilva, 2009; Latimer et al., 1987), an angle close to 90° between the long axis and distal articular surface of the tibia (DeSilva, 2009; Latimer et al., 1987), a more symmetric talar trochlea (DeSilva, 2009; Latimer et al., 1987), a relatively stiff midfoot without a midtarsal break (DeSilva, 2010; Elftman & Manter, 1935), and a complex of features, including the medial longitudinal arch, metatarsophalangeal joints, and various soft tissues, which contribute to the windlass mechanism

(Griffin, Miller, Schmitt, & D'aouit, 2015) that improves locomotor efficiency (Ker, Bennett, Bibby, Kester, & Alexander, 1987).

In part due to the mosaic nature of fossil hominin morphology, but also due to reliance on fragmentary or isolated postcranial elements, paleoanthropologists often differ in their interpretations of the functional significance of various morphological features. It remains unclear, based on the morphology of the ankle, whether early hominins continued to engage in a significant amount of arboreal behavior and whether hominin species used kinematically similar or distinct forms of bipedalism, perhaps unlike the modern human bipedal gait (e.g., Clarke & Tobias, 1995; Day & Wood, 1968; DeSilva, 2009; DeSilva et al., 2013; DeSilva & Throckmorton, 2010; Haile-Selassie et al., 2012; Harcourt-Smith & Aiello, 2004; Harcourt-Smith et al., 2015; Latimer et al., 1987; Lisowski, Albrecht, & Oxnard, 1974, 1976; Oxnard & Lisowski, 1980; Prang, 2015, 2016; Stern & Susman, 1983; Zipfel et al., 2011). Functional interpretation of the external skeletal morphology of the foot is further complicated by the role of soft tissues in limiting or enabling adoption of different foot postures (Venkataraman, Kraft, DeSilva, & Dominy, 2013; Venkataraman, Kraft, & Dominy, 2013) and by the substantial individual variability in the flexibility of the modern human foot (Bates et al., 2013; DeSilva et al., 2015). As the foot comprises a complex system of bones, tendons, ligaments and muscles, there are potentially many different ways for it to adapt to different functions, other than by modification of external bone shape (Crompton, 2015). Even modern humans are able to access numerous resources efficiently from the arboreal environment (Kraft, Venkataraman, & Dominy, 2014), without any apparent external morphological signal on the talus and distal tibia (Venkataraman, Kraft, DeSilva et al., 2013).

Analysis of internal bone structure, both cortical and trabecular bone, of the talocrural and talonavicular joint has potential to provide further insight into interpreting use of the foot in the past. While external articular morphology indicates the joint positions a species was *able* to adopt, the internal bone structure can provide information about how a joint was *actually* loaded (Kivell, 2016; Ruff & Runestad, 1992). This is because both trabecular and cortical bone structure can adapt to loading during an individual's lifetime (e.g., Barak, Lieberman, & Hublin, 2011; Kivell, 2016; Lanyon, 1974; Pontzer et al., 2006; Robling, Hinant, Burr, & Turner, 2002; Ruff, Holt, & Trinkaus, 2006), by remodeling in response to strain (Ehrlich & Lanyon, 2002). Structural adaptations can occur at the level of individual trabeculae (Cresswell, Goff, Nguyen, Lee, & Hernandez, 2015; Schulte et al., 2013). As these individual trabeculae appear able to adapt to accommodate regional strains, it is likely that regional architectural parameters can provide information about how different areas of a joint are loaded. For example, trabecular and cortical bone distribution close to the articular surface, radiodensity patterns, and indicators of bone remodeling, correspond with predicted locations of peak loading associated with specific joint positions (Carlson, Jashashvili, Houghton, Westaway, & Patel, 2013; Mazurier, Nakatsukasa, & Macchiarelli, 2010; Patel & Carlson, 2007; Polk, Blumenfeld, & Ahluwalia, 2008; Polk, Williams, Peterson, Roseman, & Godfrey, 2010; Skinner et al., 2015; Tsegai et al., 2013; Zeining, Richmond, & Hartman, 2011).

Experimentally changing the loading regime of a joint or limb by, for example, changing the angle of the joint during loading or subjecting a limb to an unnatural load, leads to predictable alterations in both cortical and trabecular bone (Barak et al., 2011; Cresswell et al., 2015; Pontzer et al., 2006; Robling et al., 2002). It is often difficult to relate bone structure, especially that of trabecular bone, directly to the biomechanical environment, i.e., to connect specific architectural variables to joint function and loading regime. Factors other than behavior have the potential to influence, or even be the main factor determining, bone form (Bertram & Swartz, 1991; Kivell, 2016; Lovejoy, McCollum, Reno, & Rosenman, 2003; Ruff et al., 2006). There is still much that we do not fully understand about bone functional adaptation, including the genetic and systemic factors that shape trabecular and cortical structure (Carlson, Lublinsky, & Judex, 2008; Havill et al., 2010; Lieberman, 1996; Paternoster et al., 2013; Tsegai, Skinner, Pahr, Hublin, & Kivell, 2016; Wallace, Kwaczala, Judex, Demes, & Carlson, 2013; Wallace et al., 2010). These include the way in which bone remodels depending upon the duration, frequency, or magnitude of the external load (e.g., Frost, 1987; Rubin & Lanyon, 1985; Skerry & Lanyon, 1995), or how these factors might vary depending on species (e.g., Turner, 2001), anatomical region (e.g., Morgan & Keaveny, 2001), age (e.g., Pearson & Lieberman, 2004) or body mass (e.g., Biewener, 1990; Doube, Klosowski, Wiktorowicz-Conroy, Hutchinson, & Shefelbine, 2011). Moreover, cortical and trabecular bone may respond differently to strain or even interact to compensate for each other (Carlson & Judex, 2007). It is likely that these factors vary between even closely related species/sub-species. For example, some of the genetic differences between modern humans and Neanderthals relate to bone growth (Green et al., 2010), and changes in indirect measures of hormone levels occur at different developmental stages in humans, chimpanzees and bonobos (e.g., TT3: Behringer, Deschner, Deimel, Stevens, & Hohmann, 2014; testosterone: Behringer, Deschner, Murtagh, Stevens, & Hohmann, 2014). All of these factors can confound our functional interpretations of variation in bone structure. However, there is a wealth of comparative, computational and in vivo research that makes clear that variation in cortical and trabecular structure reflects, at least to some degree, variation in external loading (Kivell, 2016; Ruff et al., 2006).

The hominoid foot and ankle, specifically the talocrural and talonavicular joints, are well suited to analysis of internal bone structure due to differences in foot postures adopted by modern humans and extant apes, the specific structure of the joint, and the close association of the foot with the substrate. Several studies have investigated the kinematics of the foot, during both quadrupedal and bipedal locomotion, in humans and chimpanzees (e.g., Holowka, O'Neill, Thompson, & Demes, 2017; O'Neill et al., 2015; Pontzer, Raichlen, & Rodman, 2014; Pontzer, Raichlen, & Sockol, 2009; Sockol, Raichlen, & Pontzer, 2007). As modern human bipeds and chimpanzee climbers/knuckle-walkers adopt divergent foot postures (DeSilva, 2009), the loading environment within the foot and at the ankle is likely to differ between these groups. In chimpanzees, the ankle is loaded in dorsiflexion during both vertical climbing and during quadrupedal knuckle-walking (Barak, Lieberman, Raichlen et al., 2013; DeSilva, 2009; Pontzer et al., 2009,

2014; Sockol et al., 2007), whereas the human ankle adopts a more neutral posture during bipedalism (Barak, Lieberman, Raichlen et al., 2013). The chimpanzee ankle is also inverted during climbing (DeSilva, 2009; Latimer et al., 1987; Lewis 1980a). Loading at the talonavicular joint is characterized by greater mobility in *Pan* compared to *Homo*, either related to dorsiflexion (i.e., the midtarsal break) or to rotation (DeSilva, 2010; Elftman & Manter, 1935; Thompson, Holowka, O'Neill, & Larson, 2014; but see Holowka et al., 2017). The high joint congruity between the distal tibia and the trochlea surface of the talus (Latimer et al., 1987) indicates that the bone structure is likely to be directly related to joint use, and not to other factors such as the action of muscles, as in other regions (e.g., the humeral head), where the bony articulation itself does not maintain joint integrity. In the absence of muscle/tendon attachments on the talus itself, and thus of tensile forces caused by muscle contractions, this region also offers an opportunity to analyze the effects of locomotor forces alone on trabecular bone structure (DeSilva & Devlin, 2012). Further, as the foot is in direct contact with the substrate, it directly experiences the initial forces of locomotion, unlike more proximally located joints. The same is true for the hand, where clear trabecular signals of the direction of loading are present (Skinner et al., 2015; Tsegaj et al., 2013).

Previous analyses have assessed the functional significance of trabecular and cortical bone structure of the ankle in humans (talus: Athavale, Joshi, & Joshi, 2008; Ebraheim, Sabry, & Nadim, 1999; Nowakowski, Deyhle, Zander, Leumann, & Müller-Gerbl, 2013; Pal & Routal, 1998; Schiff et al., 2007; Sinha, 1985; Takechi, Ito, Takada, & Nakayama, 1982; talus and distal tibia: Hvid, Rasmussen, Jensen, & Nielsen, 1985), and several studies have adopted a comparative approach across different taxa (talus: DeSilva & Devlin, 2012; Hérbert, Lebrun, & Marivaux, 2012; Su, 2011; Su & Carlson, 2017; Su, Wallace, & Nakatsukasa, 2013; tibia: Barak, Lieberman, Raichlen et al., 2013; Carlson, Chirchir, & Patel, 2016; Su, 2011). DeSilva and Devlin (2012) found interspecific differences in regional patterning of trabecular structure across four quadrants of the talar body but were unable to attribute these differences to locomotor mode and a biomechanical explanation remains unclear. Analysis of more localized subregions, sampling bone directly adjacent to the articular surface, has shown regional patterning of degree of anisotropy (DA), elongation and primary trabecular orientation, which is distinct in modern humans when compared with extant apes, with fossil hominins displaying some ape-like and some human-like features (Su, 2011; Su & Carlson, 2017; Su et al., 2013). At the distal tibia, the orientation of trabecular bone in humans and chimpanzees corresponds with measurements of dorsiflexion at the ankle (Barak, Lieberman, Raichlen et al., 2013). Previous studies have assessed cortical thickness and radiodensity patterns of the articular surfaces of the primate talus and distal tibia (talus: Su, 2011; tibia: Carlson et al., 2016; Su, 2011), and behavioral correlates have been identified from bone profiles and radiodensity patterns at articular surfaces of other primate and mammalian taxa and epiphyses (Carlson et al., 2013; Mazurier et al., 2010; Patel & Carlson, 2007). However, to our knowledge no previous study has comparatively analyzed cortical thickness maps in both the talus and distal tibia of humans and chimpanzees.

Previous studies quantifying trabecular bone structure and/or bone strength characteristics at the ankle relied on analyses of multiple volumes of interest (DeSilva & Devlin, 2012; Su, 2011; Su et al., 2013) or on destructive methods (Athavale et al., 2008; Sinha, 1985). Inter-specific analyses are often complicated by the difficulty in identifying biologically homologous regions, and differences in VOI size and location have a substantial impact on trabecular bone analysis, especially when comparing among species that vary greatly in size and in morphologically complex bones (Lazenby, Skinner, Kivell, & Hublin, 2011; Kivell, Skinner, Lazenby, & Hublin, 2011; Maga, Kappelman, Ryan, & Ketcham, 2006). Moreover, trabecular bone close to the articular surface, which can be difficult to sample using VOI-based methods that require manual discrimination between cortical and trabecular bone, is more likely to be of biomechanical relevance as it experiences the initial joint reaction forces, and bone closer to the articular surface differs from that in the center of the epiphysis (Singh, 1978). Analyses of bone strength at the articular surface have not investigated the cortical and trabecular structure independently but have instead used methods which quantify cortical bone and some of the underlying trabeculae (Mazurier et al., 2010; Patel & Carlson, 2007). In this study, we address some of these challenges by using two methodologies that allow independent quantification of the trabecular and the cortical structure. The trabecular bone analysis applied here enables quantification of trabecular structure throughout the bone or in a predefined region of the epiphysis, however, statistical comparisons cannot be conducted between groups. For cortical bone, we use a method that is able to compare cortical thickness across the bone/epiphysis between groups, but does not allow quantification of trabecular structure further than around 5mm beneath the cortex. By combining these complementary methodologies, we are able to analyze patterns of both cortical and trabecular bone in the human and chimpanzee talus and distal tibia. As a result, we are able to generate a fine scale, nuanced analysis through the visualization of regional patterning of both cortical and trabecular bone, which may provide detailed information about joint loading.

In this study, we measure trabecular and cortical bone of the talus and distal tibia in *Pan troglodytes verus* and *Homo sapiens*. We test the following predictions in how trabecular bone structure and distribution, and cortical thickness and distribution differ between *Pan* and *Homo*. First, as both the talocrural and talonavicular joint are used in a greater range of positions in *Pan*, and both joints are less mobile in *Homo*, we predict a higher DA in humans in both the talus and tibia (Barak, Lieberman, Raichlen et al., 2013; Su, 2011; Su & Carlson, 2017; Su et al., 2013; Thompson et al., 2014; but see Holowka et al., 2017). Second, following the findings of previous trabecular studies that sedentary modern humans have a generally low BV/TV and cortical thickness (Chirchir et al., 2015; Chirchir, Ruff, Junno, & Potts, 2017; Lieberman, 1996; Ruff, 2005; Ruff, Trinkaus, Walker, & Larsen, 1993; Ryan & Shaw, 2015; Scherf, Wahl, Hublin, & Harvati, 2015), we predict an overall lower BV/TV and thinner cortex in *Homo*. Third, we hypothesize that the regional distribution of both cortical and trabecular bone will reflect differences in habitual peak loading of the talocrural and talonavicular joints. More specifically, that at the talocrural joint *Pan*

will show a pattern of BV/TV and cortical thickness that reflects use of the foot in dorsiflexion and inversion, and at the talonavicular joint a greater degree of mobility. In *Homo*, the trabecular bone distribution and cortical thickness will reflect less mobility, and a more neutral ankle position.

2 | MATERIALS AND METHODS

2.1 | Sample

This study analyzed trabecular and cortical bone morphology of the tibia and talus of two species with divergent modes of locomotion: *P. troglodytes verus* and *H. sapiens*. The sample, detailed in Table 1, included fifteen wild *P. troglodytes verus* individuals (tibiae: $N = 10$; tali: $N = 13$; of which $N = 8$ were paired) whose skeletal remains were collected from the Taï National Park, Cote d'Ivoire, and ten *H. sapiens* individuals (tibia: $N = 8$; tali: $N = 9$; of which $N = 7$ were paired) from an 18th to 19th century cemetery in Inden, Germany. Adult specimens were used, based on fusion of the epiphyses throughout the skeleton and no external signs of pathology or senescence related changes were present. The right side was chosen where both talus and tibia were available and free from damage, otherwise the left side was used.

2.2 | Computed tomography

High resolution micro-computed tomography (CT) scans were collected with a BIR ACTIS 225/300 CT scanner for the tibiae and with a Sky-Scan1173 CT scanner for the tali, using an acceleration voltage of 130 kV and 100 μ A and either a 0.5 mm brass or 1 mm aluminum filter, at the Department of Human Evolution, Max Planck Institute for Evolutionary Anthropology (Leipzig, Germany). Isotropic acquisition voxel sizes were 25–36 μ m for the tibia and talus of *Homo* and 19–30 μ m for the tibia and talus of *Pan*. Each scan was reconstructed as a 2,048 \times 2,048 16-bit TIFF image stack from 2,500 projections with three-frame averaging. Following reconstruction, all specimens were reoriented into standardized positions using AVIZO 6.3® (Visualization Sciences Group, SAS) and segmented using a Ray Casting Algorithm (Scherf & Tilgner, 2009).

Prior to segmentation, all *Pan* specimens were resampled to 35 μ m and all *Homo* specimens to 40 μ m, due to processing constraints. The relative resolutions, a measure of how adequately the average trabecular strut is represented (i.e., mean trabecular thickness [mm]/resolution [mm]), are shown in Table 1. The average for the entire sample of 7.57

(range: 5.46–11.59) is consistent with previous studies of trabecular bone structure (Kivell et al., 2011; Sode, Burghardt, Nissenson, & Majumdar, 2008; Tsegaj et al., 2013), and is appropriate for microstructural analysis.

2.3 | Analysis of trabecular bone microstructure

To quantify trabecular bone, each material in the scan (Figure 1a), i.e., cortical bone, trabecular bone, air and the internal bone cavity, were segmented automatically using an in house script in medtool v3.9 (www.dr-pahr.at), following Gross, Kivell, Skinner, Nguyen, and Pahr (2014). Morphological filters were used to separate these regions, and the kernel size used was adjusted for each individual according to its measured trabecular thickness, enabling an accurate, subject-specific segmentation. This resulted in three data sets that were used in subsequent processing steps: (a) the trabecular bone (Figure 1b), (b) the inner region of the bone, and (c) the inner mask (Figure 1c), which contains the internal region of the bone where internal bone cavity and trabecular bone are represented by different grey values and the cortex has been removed. This automated segmentation was problematic in two locations in the talus, at the inferior talar neck and at the subtalar joint surfaces, due to their complex morphology. Thus the results from these regions are treated with caution. The proximal boundary of the distal tibia was defined as the point at which curvature of the shaft begins in both medial and anterior views, which is at the proximal extent of the fibular notch, and is an equivalent location across the sample.

From the trabecular only mask (Figure 1b), trabecular thickness (Tb.Th), bone surface area (BS), and bone volume (BV) were quantified using the BoneJ plugin (version 1.3.12; Doube et al., 2010) for ImageJ v1.46r (Schneider, Rasband, & Eliceiri, 2012). Bone surface to volume ratio (BS/BV) was subsequently calculated.

The inner region of the bone was used to create a 3D tetrahedral mesh with a mesh size of 1mm, using CGAL 4.4 (CGAL, Computational Geometry, <http://www.cgal.org>). The inner mask (Figure 1c) was used to calculate BV/TV throughout the bone to generate 3D color maps of bone distribution, and to calculate the overall bone volume fraction (BV/TV) and DA using medtool v3.9. A rectangular background grid, with a grid size of 2.5 mm, was applied and a spherical VOI with a diameter of 5 mm was used to measure BV/TV at each node of the grid. A sphere size of 5 mm is appropriate as enough trabecular struts are sampled to adequately quantify trabecular parameters (Gross et al., 2014). To create a 3D color map of bone distribution, the BV/TV values at each node were interpolated to assign each element in the 3D

TABLE 1 Study sample

Taxon	Body mass (kg) ^a	Locomotor behavior	Tibia	Talus	Paired	Scan resolution (μ m)	Relative resolution ^b
<i>Homo sapiens</i> ^c	62.1–72.1	Biped	8	9	7	40	5.72–9.06
<i>Pan troglodytes verus</i> ^d	41.6–46.3	Arboreal/ knuckle-walker	10	13	8	35	5.46–11.59

^aSex specific mean body mass (F-M). Body masses from Smith and Jungers (1997). ^bRelative resolution = mean trabecular thickness (mm)/resolution (mm). ^cAnthropological Collection of Institute of Zoology and Anthropology, University of Göttingen. ^dMax Planck Institute for Evolutionary Anthropology.

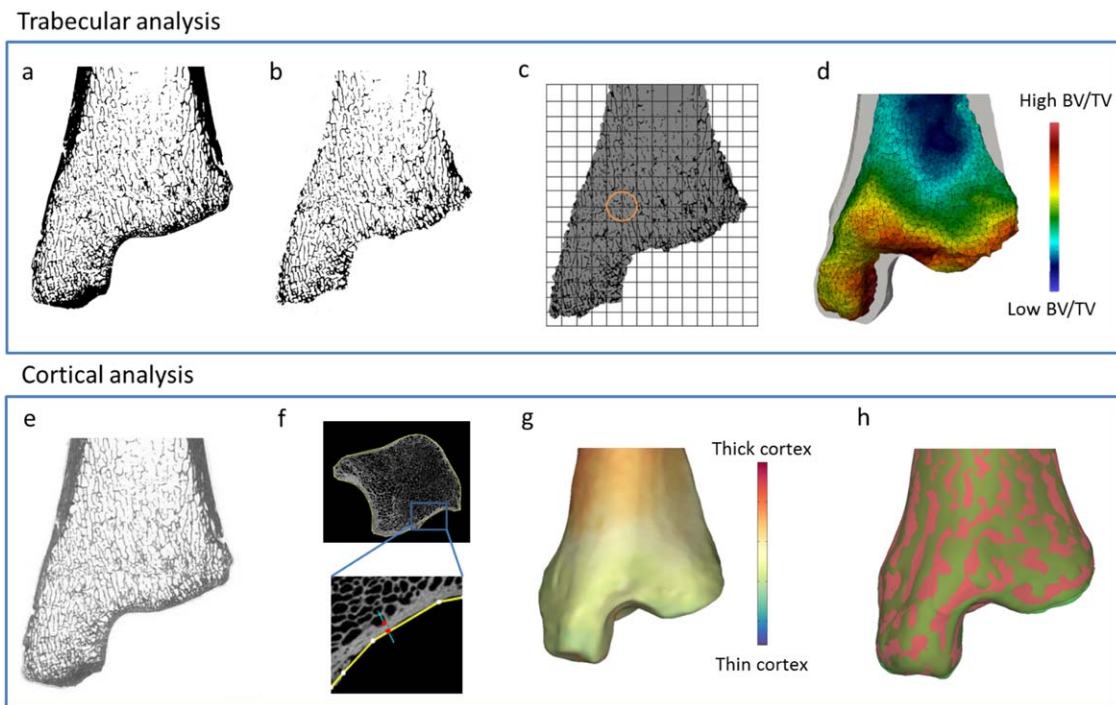


FIGURE 1 Processing steps for trabecular and cortical bone analysis for a *Pan* distal tibia. (a) Segmented microCT scan. (b) Segmented trabecular bone. (c) Inner mask, where trabecular bone and internal region of the bone are assigned different grey values, and the cortical bone has been removed. A background grid and sampling sphere are applied to calculate trabecular structure throughout the bone. (d) Tetrahedral mesh with color scalars representing trabecular bone volume fraction. (e) Unsegmented voxel data. (f) Process of measurement of cortical thickness. (g) Cortical thickness values mapped to a subject-specific surface. (h) Each subject-specific surface (green) is registered to a canonical surface (red) for interspecific comparisons

mesh of the trabecular region a BV/TV value (Figure 1d). The color maps were visualized in Paraview v4.0.1 (Ahrens, Geveci, & Law, 2005). The overall BV/TV value was calculated as the mean of the values for each element in the 3D mesh, and thus is the average for the whole bone/epiphysis. The mean intercept method (Odgaard, 1997; Whitehouse, 1974) was used to calculate the mean fabric tensor, the arithmetic mean of all second order fabric tensors normalized using the determinants. The extracted eigenvalues and eigenvectors were then used to calculate the DA ($DA = 1 - [\text{smallest eigenvalue}/\text{largest eigenvalue}]$), whereby a DA of 1 indicates complete anisotropy and a DA of 0 complete isotropy.

2.4 | Analysis of cortical bone microstructure

To compare cortical thickness between *Pan* and *Homo* in the talus and distal tibia, cortical bone thickness maps were generated for each specimen (following Treece, Gee, Mayhew, & Poole, 2010; Treece, Poole, & Gee, 2012; Tsegai et al., 2017). This was accomplished via semiautomatic segmentation of the cortical surface, from the unsegmented CT data (Figure 1e,f) in Stradwin v5.1a (Treece, Gee, Cambridge; <http://mi.eng.cam.ac.uk/~rwp/stradwin>). Following definition of the surface, around 15,000 independent measurements of cortical thickness were calculated throughout the bone (Figure 1f) and mapped onto a subject-specific surface (Figure 1g). Subsequently, each surface was registered to a canonical surface using wxRegSurf v13 (Figure 1h). The canonical surface used was an average of the entire sample, each species was

averaged separately and then the average of the two resulting surfaces was used, to prevent the difference in sample size affecting the average morphology. After registration to the canonical surface, mean thickness maps were generated for each species.

2.5 | Statistical analysis

For trabecular bone analysis, all statistical tests were performed using R v3.0.3 (R Core Team, 2016) and ggplot2 was used for generating plots (Wickham, 2009). Shapiro-Wilk test for normality showed that the data were not normally distributed and thus nonparametric tests were used. Mann-Whitney *U* tests were used to test for statistical differences in trabecular bone parameters between *Homo* and *Pan*. A principal component (PC) analysis was conducted to determine which parameters contributed to interspecific differences in the talus and in the tibia. All variables were included in the PC analysis: Tb.Th, BV/TV, DA, BS/BV, and cortical thickness. As there are large differences in the variances of these variables, prior to analysis the data was centered and scaled to unit variance. PCs were subsequently derived by singular value decomposition of the resulting data matrix. Spearman's correlation test and RMA regression were used to test for correlation between trabecular parameters and cortical thickness in the talus and distal tibia. To test the relationship between size and trabecular bone parameters, OLS \log_{10} regressions and Pearson's correlation tests were conducted for each trabecular parameter against the size of the epiphysis/bone for each taxon. The size of each bone was represented as

the geometric mean of several measurements, both of overall bone size and of the size of the articular surfaces. For the talus, these measurements were the anteroposterior length, mediolateral width and dorsoplantar height of the talus, the anteroposterior length and mediolateral width of the talar trochlea, and the dorsoplantar height and mediolateral width of the talar head. For the tibia, a geometric mean was derived from the maximum anteroposterior length and maximum mediolateral width of the distal tibia, the anteroposterior length and mediolateral width of the distal articular surface, the anteroposterior length, mediolateral width, and proximodistal height of the medial malleolus. Pearson's correlation test was used to compare trabecular parameters between paired tibia and tali in each taxon. Statistical parametric mapping was used to identify regional cortical thickness differences between the two species (Friston et al., 1995), using the SurfStat package (Worsley et al., 2009), by fitting a general linear model (GLM) to the data. This model determined whether cortical thickness differences could be explained by species (covariates of interest) or other factors (confounding covariates). As there is risk of systematic misregistration due to shape differences, nonrigid shape coefficients were included as confounds in the GLM (Gee & Treece, 2014; Gee, Treece, Tonkin, Black, & Poole, 2015). Bone size, however, was strongly correlated with species and therefore not included as a confound in the GLM. Statistical parametric maps were generated using F statistics and the corresponding p -values were corrected for multiple comparisons using random field theory to control for the chance of false positives. Relative cortical thickness was calculated for each specimen, by subtracting the individual mean value from each individual thickness measurement and dividing by the standard deviation. In this way, relative patterns of cortical thickness could be analyzed, despite considerable interspecific differences in absolute cortical thickness. For all statistical tests, a p -value of <0.05 was considered significant.

3 | RESULTS

3.1 | Trabecular and cortical architecture of the talus and tibia

Means and standard deviations of measured trabecular and cortical parameters and Mann-Whitney U -test results are shown in Table 2, and extracted regions of trabecular bone, visualizing structural differ-

ences, are shown in Figure 2. Mann-Whitney U -test results (Table 2) find that the trabecular structure of *Pan* differs from that of *Homo* in having a significantly greater BV/TV and lower BS/BV in both the talus and the tibia. The trabecular structure is more divergent in the talus than in the tibia: with the talus of *Pan* having significantly thicker, less uniformly oriented trabeculae (i.e., lower DA). The cortex of *Pan* is significantly thicker in both the talus and the tibia compared to *Homo*.

Correlations between parameters in the talus and tibia of each taxon are reported in Table 3. Significant correlations between variables differ both between taxa and between skeletal regions. As such, all parameters were included in the analysis, although correlations between parameters may lead to overemphasis of the contribution of these variables. Table 4 shows the results of the PC analysis, and Figure 3 shows the plot of PC1 against PC2 for both the talus and tibia. Together, PC1 and PC2 explain 92.90% and 90.85% of the variance for the talus and tibia, respectively and in both analyses, *Homo* and *Pan* are clearly separated. All four trabecular parameters and cortical thickness contribute equally to PC1 in the talus, distinguishing *Pan*, with greater BV/TV, Tb.Th and cortical thickness, but lower DA and BS/BV, from *Homo*. PC2 is driven by Tb.Th and BS/BV, but only separates out particular individuals within each taxon. In the tibia, separation along PC1 is largely determined by BV/TV, BS/BV and cortical thickness. Along PC2, most *Pan* individuals are distinguished from *Homo* in having lower Tb.Th and higher DA.

3.2 | Allometry

The results of the \log_{10} OLS regressions of each parameter against the geometric mean, a proxy for bone size, are shown for *Pan* and *Homo* in Table 5 and Figures 4 and 5. There were no significant correlations between any trabecular parameter and bone size. However, the relationship between size and trabecular and cortical structure does differ between species and between the talus and tibia (Figures 4 and 5).

3.3 | Correlation between the talus and tibia

Paired tali and tibiae were used to compare trabecular and cortical bone parameters between the talus and tibia in seven *Homo* and eight *Pan* specimens (Table 6 and Figure 6). Within *Pan*, all parameters other than DA are strongly correlated across the joint (i.e., $r > 0.70$), whereas in *Homo*, only Tb.Th and BS/BV are strongly and significantly correlated.

TABLE 2 Mean and standard deviation of trabecular and cortical parameters in the talus and distal tibia of *Homo* and *Pan*

Element	Taxon	Tb.Th (mm)	BV.TV (%)	DA	BS/BV (mm^{-1})	Cortical thickness (mm)
Talus	<i>Homo</i>	0.26 (0.03)	24.77 (2.17)	0.14 (0.07)	0.32 (0.05)	0.45 (0.06)
	<i>Pan</i>	0.31 (0.04)	34.65 (2.63)	0.02 (0.02)	0.19 (0.02)	0.88 (0.19)
	Significance	<0.01	<0.01	<0.01	<0.01	<0.01
Tibia	<i>Homo</i>	0.25 (0.04)	19.92 (2.87)	0.29 (0.10)	0.45 (0.08)	0.63 (0.07)
	<i>Pan</i>	0.23 (0.02)	24.17 (3.43)	0.32 (0.06)	0.31 (0.06)	1.13 (0.19)
	Significance	0.17	0.02	0.51	<0.01	<0.01

Note. Results of Mann-Whitney U test between taxa are shown, with significant differences in bold.

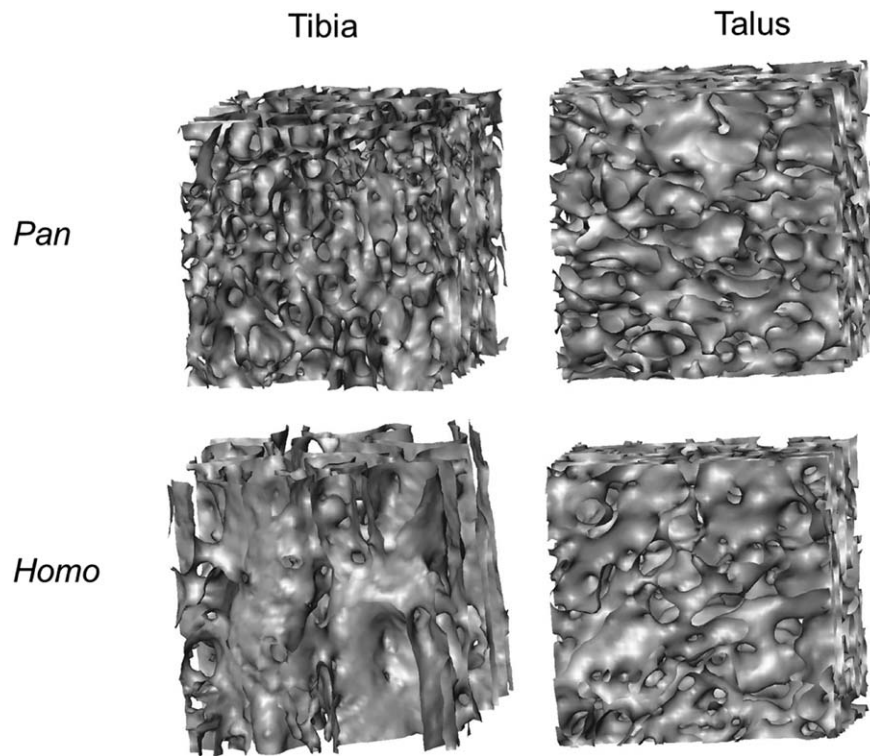


FIGURE 2 Extracted cubes of trabecular bone from approximately the same location in the talus and distal tibia of *Homo* and *Pan*

3.4 | Distribution of trabecular bone in the talus and distal tibia

Figure 7 shows BV/TV color maps for the talus of one representative individual of *Homo* and *Pan*. Images of the full sample are included in the Supporting Information.

On the dorsal surface of the talus (Figure 7a,f), all *Pan* specimens share a region of high BV/TV on the lateral edge of the trochlea. In some individuals this extends posteriorly along the edge, and in others it is more anteriorly confined. Some, but not all, specimens have an additional region of higher BV/TV on the medial trochlea, which is not consistent in its location or anteroposterior extent (see Supporting Information). In *Homo*, there is no consistent pattern of trabecular bone distribution on the dorsal surface of the trochlea as this region is highly variable across the sample. All individuals of both *Pan* and *Homo* have a region of high BV/TV on the dorsal surface of the talar neck, although this is much more pronounced in *Pan*. In a transverse plane, where the superior portion of the talus has been removed (Figure 7b, g), there is a region of high BV/TV at the neck in *Pan*, although, as mentioned above, the inferior region of the neck must be interpreted with a certain degree of caution due to problems segmenting trabeculae from cortex. In *Homo*, there is no localized region of high BV/TV in the neck, but instead an anteroposterior trajectory of bone running through the head and neck, which is absent in *Pan*. The region of high BV/TV at the articular surface of the talar head (i.e., at the talonavicular joint), is more localized in *Homo* than in *Pan*. This is clearly seen in anterior view (Figure 7c,h), where *Homo* has a point of high BV/TV located dorsally on the head, in contrast to *Pan*, where there is a band running mediolaterally across the head. In the coronal (Figure 7d,i) and sagittal

(Figure 7e,k) planes of *Homo*, the center of the talar body contains a relatively higher BV/TV than in *Pan*. Also, in the sagittal plane (Figure

TABLE 3 Results of Spearman's correlation test to test relationship between trabecular parameters within *Homo* and *Pan* in the talus and distal tibia

Element	Taxon	Parameter	Tb.Th	BV/TV	BS/BV	DA
Talus	<i>Homo</i>	BV/TV	0.42	-		
		BS/BV	-0.18	-0.92**	-	
		DA	-0.82**	-0.45	0.28	-
		CTh	0.57	0.50	-0.30	-0.72*
	<i>Pan</i>	BV/TV	0.59*	-		
		BS/BV	-0.10	-0.80**	-	
		DA	-0.98**	-0.66**	0.16	-
		CTh	0.84**	0.63*	-0.24	-0.80**
Tibia	<i>Homo</i>	BV/TV	0.71	-		
		BS/BV	-0.83**	-0.90**	-	
		DA	-0.74*	-0.50	0.69	-
		CTh	0.31	0.07	-0.07	-0.02
	<i>Pan</i>	BV/TV	0.75*	-		
		BS/BV	-0.67*	-0.95**	-	
		DA	-0.71*	-0.62	0.41	-
		CTh	0.82**	0.65*	-0.66*	-0.44

Note. Significant differences reported in bold with * $p < 0.05$; ** $p < 0.01$. CTh, cortical thickness.

TABLE 4 Results of principal component analyses showing percentage variance and loading for each principal component

Element	Parameter	PC1	PC2	PC3	PC4	PC5
Talus	% variance (cumulative)	82.64 (82.64)	10.27 (92.90)	4.35 (97.26)	2.43 (99.69)	0.31 (100.00)
	Tb.Th	0.41	0.70	0.30	0.50	-0.08
	BV/TV	0.48	-0.28	0.09	0.08	0.82
	DA	-0.44	-0.21	0.85	0.16	0.07
	BS/BV	-0.43	0.62	-0.05	-0.40	0.51
	Cortical thickness	0.46	0.05	0.41	-0.75	-0.22
Tibia	% variance (cumulative)	56.45 (56.45)	34.41 (90.85)	5.41 (96.26)	2.88 (99.14)	0.86 (100.00)
	Tb.Th	0.27	-0.65	0.03	-0.71	-0.06
	BV/TV	0.57	0.13	0.42	0.06	0.69
	DA	-0.30	0.62	0.29	-0.67	0.02
	BS/BV	-0.55	-0.22	-0.36	-0.09	0.72
	Cortical thickness	0.46	0.37	-0.78	-0.20	0.05

Note. The analysis was conducted separately for the talus and tibia, including Tb.Th, BV/TV, DA, BS/BV, and cortical thickness. High loadings (i.e., greater than 0.40) are shown in bold.

7e,k) there is a distinct trajectory of high BV/TV running anteroposteriorly through the talar head of *Homo* that is not found in *Pan*. Instead, the *Pan* neck has a region of high BV/TV on the dorsal surface. Comparison of the individual BV/TV scales shows that *Pan* has a higher BV/TV than *Homo* in both its minimum and maximum values.

Color maps of the BV/TV distribution in the distal tibia of *Homo* and *Pan* are shown in Figure 8 and results for the entire sample are included in the Supporting Information. On the distal articular surface of the tibia (Figure 8a,e), some specimens of *Homo* have a high concentration of BV/TV confined to the medial side of the articular surface and in other individuals it is centrally located. This is in contrast to *Pan*, where there are consistently three regions of higher BV/TV: anterolateral, anteromedial and posterocentral. When viewed in the midsagittal plane of the distal tibia (Figure 8b,f), the anteromedial and posterior concentrations of bone are visible in *Pan*, in contrast to the more central and continuous area of high BV/TV in *Homo*. On the anterior edge of the distal tibia (Figure 8c,g), *Pan* has a high concentration of bone extending

across the edge that is absent in *Homo*. In the midcoronal plane (Figure 8d,h), *Pan* contains a relatively greater BV/TV in the center of the medial malleolus, compared to *Homo*. Unlike the talus, the range of BV/TV is more similar between the two species (Figures 7 and 8, scale bars).

3.5 | Distribution of cortical bone in the talus and distal tibia

Mean relative cortical thickness maps for the talus and distal tibia of *Pan* and *Homo*, along with regions of significant differences, are shown in Figures 9 and 10. In contrast to the trabecular bone maps, these figures do not show the cortical thickness in just one individual, but rather the mean of all individuals by taxon. As *Pan* has a greater cortical thickness in both the talus and the distal tibia, results are presented for relative cortical thickness values, equalized by subtracting the mean value from each cortical thickness value and dividing by the standard deviation for every individual in the sample.

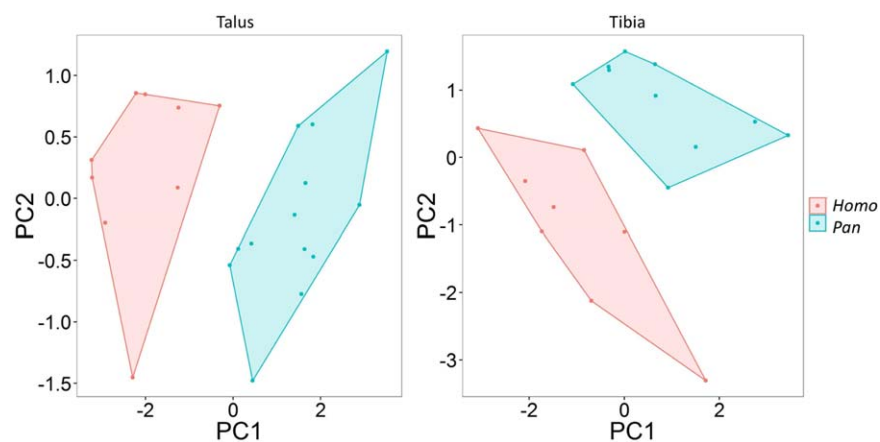


FIGURE 3 PC1 and PC2 for trabecular and cortical structure of the talus and distal tibia of *Pan* (blue) and *Homo* (red)

TABLE 5 The relationship between bone structure and bone size in *Homo* and *Pan*

Taxon	Element	Parameter	Pearson's <i>r</i>	Slope	Lower 95% CI	Upper 95% CI	<i>p</i> -value	<i>R</i> ²
<i>Homo</i>	Talus	Tb.Th	-0.40	-0.51	-1.58	0.57	0.30	0.15
		BV/TV	-0.48	-0.52	-1.37	0.34	0.20	0.23
		DA	0.10	2.01	-4.28	8.29	0.48	0.08
		BS/BV	0.33	0.59	-1.23	2.41	0.47	0.08
		CTh	0.12	0.23	-1.23	1.70	0.72	0.02
	Tibia	Tb.Th	0.27	0.53	-1.47	2.53	0.54	0.07
		BV/TV	0.55	1.11	-0.57	2.80	0.16	0.30
		DA	0.09	-0.05	-6.71	6.61	0.99	0.00
		BS/BV	-0.51	-1.35	-3.56	0.87	0.19	0.27
		CTh	0.25	0.38	-1.19	1.95	0.57	0.06
<i>Pan</i>	Talus	Tb.Th	0.29	0.55	-0.79	1.89	0.39	0.07
		BV/TV	-0.05	-0.06	-0.88	0.76	0.87	0.00
		DA	-0.11	-2.97	-11.57	5.62	0.46	0.05
		BS/BV	0.12	0.25	-1.15	1.65	0.70	0.01
		CTh	0.19	0.60	-1.55	2.75	0.55	0.03
	Tibia	Tb.Th	0.37	0.74	-0.64	2.11	0.25	0.16
		BV/TV	0.05	0.16	-1.70	2.03	0.84	0.01
		DA	-0.35	-1.22	-3.98	1.54	0.34	0.11
		BS/BV	-0.04	-0.04	-3.36	3.27	0.98	0.00
		CTh	0.28	0.80	-1.32	2.93	0.41	0.09

Note. Results of OLS regression and Pearson's correlation for each trabecular parameter and cortical thickness (CTh) against the geometric mean of several measurements, used as a proxy for bone size.

Visual comparison between the relative cortical thickness maps of the talus in *Homo* (Figure 9a) and *Pan* (Figure 9b), show that the regions of thickest cortical bone differ between the two species. On the talar head, *Homo* has a dorsally located region of highest relative thickness, whereas in *Pan* the region of high thickness runs mediolaterally along the dorsal half of the articular surface. At the trochlea, *Pan* has a higher cortical thickness on the lateral edge, whereas in *Homo* it is the centro-medial region that has the highest mean thickness. *Pan* and *Homo* share thick cortical bone around the region of the talar neck, however, in *Pan* this extends around the entire dorsal region of the neck, whereas in *Homo* it is confined to the dorsolateral side. In *Homo* the center of the posterior subtalar articular surface has the thickest cortical bone, whereas in *Pan* the cortical bone is thickest anterolaterally on this articular surface. Differences between *Pan* and *Homo* are shown in Figure 9c, and regions where these differences reach significance are shown in Figure 9d. There are several regions with significant differences located at the articular surfaces of the talus. *Pan* has relatively thinner bone compared to *Homo* on the anterior surface of the talar head, on the anteromedial region of the talar trochlea and on the dorsal edge of the talar head, and relatively thicker bone compared to *Homo* in a band anterolaterally on the posterior subtalar articular surface.

Cortical thickness maps, showing relative cortical thickness are shown for *Homo* and *Pan* in Figure 10a,b, respectively. In distal view, *Homo* has

thickest cortical bone the along the medial edge of the distal articular surface and the distal end of the medial malleolus. Both taxa share regions of thicker cortical bone on the distal end of the medial malleolus and the medial edge of the distal articular surface. This region on the medial articular surface is relatively thicker anteriorly in *Pan*, whereas in *Homo* this feature extends along the medial border of the articular surface. *Pan* has two additional regions of thicker cortical bone on the anterolateral and posterocentral regions of the distal articular surface. Comparisons of relative cortical thickness values between *Homo* and *Pan* are shown in Figure 10c and regions with significant differences are shown in Figure 10d. At the distal articular surfaces, *Pan* has significantly thicker cortex at the antero-medial corner, extending along the anteromedial edge of the medial malleolus. There is significantly thicker cortical bone on the distal surface of the medial malleolus in *Pan* compared to *Homo*.

4 | DISCUSSION

We analyzed the internal bone structure of the talus and distal tibia in bipedal *Homo* and arboreal, quadrupedal *Pan*. We find that trabecular and cortical bone, both the measured parameters and the regional distribution of bone, differ, often significantly, between the two taxa in ways that are potentially related to variation in joint position and load distribution

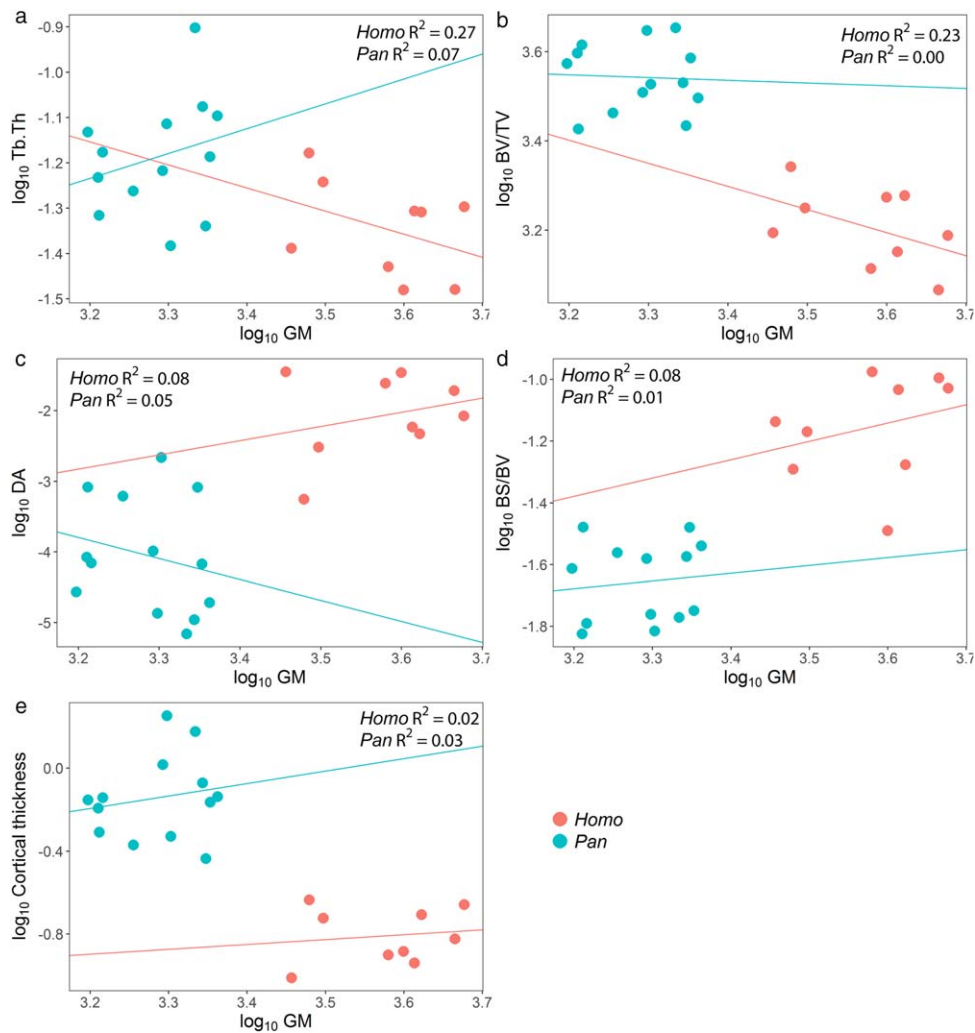


FIGURE 4 Relationship between talus size and trabecular and cortical parameters in *Pan* (blue) and *Homo* (red). The \log_{10} OLS regression lines are shown independently for *Pan* (blue) and *Homo* (red)

during locomotion. In addition to these differences, we find further support for previously proposed systemically weaker trabecular and cortical bone in recent humans (Chirchir et al., 2015, 2017; Lieberman, 1996; Ruff, 2005; Ruff et al., 1993; Ryan & Shaw, 2015; Scherf et al., 2015).

4.1 | Identifying functional signals in internal bone structure

The relationship between bone form and mechanical loading is complex. It may be influenced by numerous factors that affect bone growth and structure, which are likely to differ systematically between species and, as such, bone structure should be considered within the broader context of what is already known about the bone architecture of each species. In both the talus and distal tibia of *Homo*, we find support for our prediction that bone is relatively weak, having a lower BV/TV, a higher BS/BV and thinner cortices, compared with the more robust *Pan*. BV/TV is the strongest predictor of trabecular bone stiffness, or Young's modulus; it alone explains 87–89% of variance in stiffness (Maquer, Musy, Wandel, Gross, & Zysset, 2015; Stauber, Rapillard, van

Lenthe, Zysset, & Müller, 2006). Cortical bone thickness is also related to bone strength, as thin cortices are associated with increased fracture risk (Augat & Schorlemmer, 2006). The difference in trabecular BV/TV and cortical thickness between *Pan* and *Homo* is consistent with previous findings for the talus and distal tibia (talus: DeSilva & Devlin, 2012; Su, 2011; Su & Carlson, 2017; tibia: Barak, Lieberman, Raichlen et al., 2013; Su, 2011), and with the trabecular morphology of other anatomical regions (e.g., third metacarpal: Tsegaj et al., 2013; calcaneus: Maga et al., 2006; Zeininger, Patel, Zipfel, & Carlson, 2016; first and second metatarsal: Griffin et al., 2010; systemic: Chirchir et al., 2015). As the biomechanical environment of different joints in the human and chimpanzee are likely to vary given their divergent modes of locomotion, this consistent difference across several anatomical sites may be part of a systemic pattern (i.e., in all regions of the skeleton) and not due to specific locomotor, or other, behavior. This gracility of the modern human skeleton may be associated with increased sedentism following the adoption of agriculture, as early hominins and recent hunter-gatherers/foragers have a more robust skeleton (Chirchir et al., 2015; Lieberman, 1996; Ruff, 2005; Ruff et al., 1993; Ryan & Shaw, 2015; Scherf

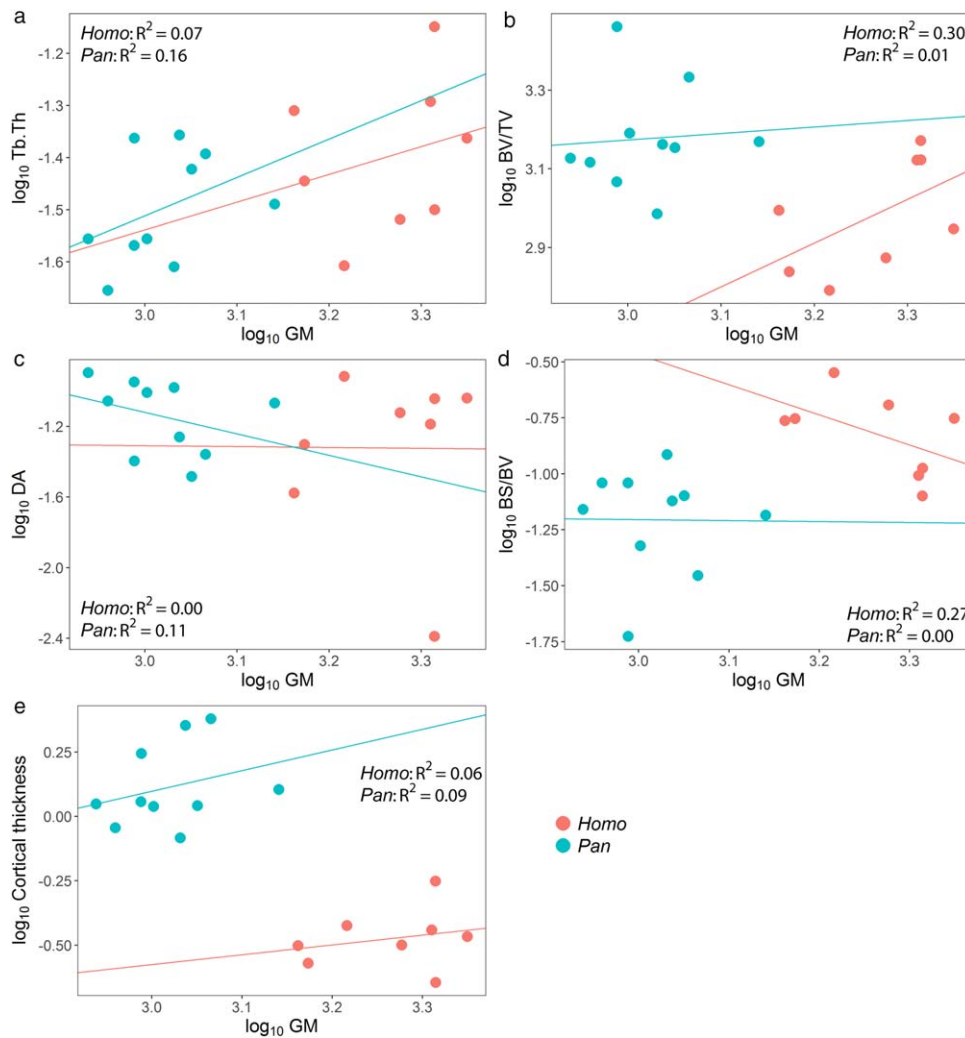


FIGURE 5 Relationship between tibia size and trabecular and cortical parameters in *Pan* (blue) and *Homo* (red). The \log_{10} OLS regression lines are shown independently for *Pan* (blue) and *Homo* (red)

et al., 2015). Analysis of the relationship between these structural parameters and size are limited by small sample sizes.

There are aspects of bone structure that appear likely to reflect joint function and thus can be of use for reconstructing behavior in the fossil record. Here, we find support for our prediction that the human talus has a significantly higher DA than in *Pan*. However, contrary to our predictions, we find no significant difference for the distal tibia. During human bipedalism the midfoot forms a relatively rigid lever during push off (Morris, 1977), compared with the flexibility of the chimpanzee midfoot (Elftman & Manter, 1935; Susman, 1983; Thompson et al., 2014; but see Holowka et al., 2017). There is also less mobility at the ankle of *Homo* than in *Pan* (Latimer et al., 1987). The less aligned trabeculae of the *Pan* talus are consistent with being more able to withstand forces from multiple directions associated with a wider range of joint positions, whereas the more highly aligned trabecular structure of the *Homo* talus appears to reflect more stereotypical loading (DeSilva & Devlin, 2012; Su, 2011; Su & Carlson, 2017; Su et al., 2013). In contrast to previous studies (Barak, Lieberman, Raichlen et al., 2013; Su, 2011), we do not find a higher DA in the distal tibia of *Homo*, but rather higher (although

not significantly so) mean DA in *Pan*. However, Su (2011) found that trabeculae in *Homo* were significantly more uniformly aligned in the talus compared with the tibia, suggesting that more similar DA values in the *Homo* and *Pan* distal tibia are not unexpected.

DA may hold a functional signal for different types of behavior that engender more or less stereotypical loads at a joint. Regional differences in DA have been useful in distinguishing between primate locomotor groups, with the structure of the proximal femur being consistent with inferred differences in loading in leaping and slow climbing strepsirrhines (Ketcham & Ryan, 2004; MacLatchy & Müller, 2002; Ryan & Ketcham, 2002a,b). The trabecular structure of the human foot is generally more highly aligned than other apes (first and second metatarsal: Griffin et al., 2010; calcaneus: Maga et al., 2006; Zeininger et al., 2016; but see Kuo, DeSilva, Devlin, McDonald, & Morgan, 2013; talus: Su, 2011; Su & Carlson, 2017; Su et al., 2013). It seems unlikely that this would relate to differences in activity level between the taxa, and there are no consistent differences in DA in the proximal femur (Ryan & Shaw, 2015) or humerus (Scherf et al., 2015) between human populations with different activity levels (i.e., engaging in the same behaviors but at different frequencies).

TABLE 6 Results of Pearson's correlation test to test relationship of each trabecular parameter and cortical thickness between the talus and distal tibia in *Homo* and *Pan*

Taxa	Parameter	Pearson's <i>r</i>	<i>p</i> -value
<i>Homo</i>	Tb.Th	0.83	0.02
	BV/TV	0.72	0.07
	DA	0.55	0.20
	BS/BV	0.83	0.02
	Cortical thickness	0.43	0.33
<i>Pan</i>	Tb.Th	0.86	0.01
	BV/TV	0.80	0.02
	DA	0.56	0.15
	BS/BV	0.81	0.02
	Cortical thickness	0.92	<0.01

Note. Significant correlations are shown in bold ($p < .05$).

Adult trabecular structure could reflect individual or interspecific differences in loading during puberty, at a time when bone is more responsive to strain (e.g., Pettersson, Nilsson, Sundh, Mellström, & Lorentzon, 2010; for cortical bone see Pearson & Lieberman, 2004). However, homologous regions of trabecular bone in adolescent and adult humans have not been sampled, as many studies exploring ontogeny have investigated changes in structure between nonadult groups (Gosman & Ketcham, 2009; Raichlen et al., 2015; Ryan & Krovitz, 2006; Ryan, van Rietbergen, & Krovitz, 2007). DA in the proximal tibial metaphysis and in the ilium continue to change between adolescence and adulthood (Abel & Macho, 2011; Gosman & Ketcham, 2009). Moreover, chimpanzees reach adult-like locomotor behavior by adolescence (Doran, 1992; Sarringhaus, MacLatchy, & Mitani, 2014), while humans reach this point during early childhood (e.g., Beck, Andriacchi, Kuo, Fermier, & Galante, 1981; Raichlen et al., 2015; Sutherland, Olshen, Cooper, & Woo, 1980). Trabecular orientation in the talus also shows plasticity later in life, as degeneration of articular cartilage, i.e., changes at the joint surface that affect loading, is associated with differences in trabecular orientation in humans (Schiff et al., 2007). This indicates that DA in adult humans and chimpanzees is likely to reflect adult behavior patterns, as loading from locomotion has remained generally consistent during much of the later growth period. Together these results suggest that the high degree of trabecular alignment throughout several elements of the human foot may be a behavioral signal related to the stereotypical loading of terrestrial bipedality. We suggest that, using our methodology, DA may provide functional information about loading in the talus, but not the tibia.

4.2 | The relationship between joint position and bone distribution

We predicted that differences in the cortical and trabecular bone distribution maps would reflect variation in dorsiflexion and inversion of the talocrural joint and the degree of mobility at the talonavicular joint.

The color maps of cortical and trabecular bone support some, but not all, of these predictions. These results are based on mean cortical thickness distribution maps and significant differences, and on BV/TV distribution maps for each individual. Generation of mean morphometric maps for BV/TV was not conducted due to the complexity of registering 3D meshes while ensuring homology.

4.2.1 | Dorsiflexion

Dorsiflexion at the ankle is characteristic of both climbing and knuckle-walking in chimpanzees compared to the more neutral ankle posture adopted by humans during bipedalism. We find no clear signal of dorsiflexion in trabecular and cortical bone of the talar trochlea but are able to identify differences in internal bone structure of the distal tibia that we propose are related to degree of dorsiflexion. In chimpanzees, during knuckle-walking the angle between the long axis of the tibia and the foot is 75.2°, compared with 85.6° in normal human bipedalism (Barak, Lieberman, Raichlen et al., 2013). During vertical climbing the degree of dorsiflexion is much greater, with an angle between the long axis of the tibia and the foot of 44.5° (DeSilva, 2009). The external morphology of the talar trochlea and the distal articular surface of the tibia is associated with this difference in loading of the ankle (DeSilva, 2009; but see Venkataraman, Kraft, DeSilva et al., 2013). It might be expected that the distribution of trabecular bone and cortical bone in the talar trochlea of *Pan* would be more anteriorly distributed, reflecting this difference in joint angle. However, we find no clear signal across the study sample in either the trabecular or cortical bone distribution maps. This is consistent with previous studies that did not identify differences in BV/TV across quadrants of the talar body (DeSilva & Devlin, 2012), or higher BV/TV and cortical thickness in the anterior talar trochlea (Su, 2011; Su & Carlson, 2017).

In contrast to the talus, we did find that the trabecular and cortical bone structure of the distal tibia reflected the differences in joint position between *Homo* and *Pan*. *Pan* shows two regions of higher BV/TV and thicker cortical bone, located at the anterior portion of the distal articular surface of the tibia, one lateral and one medial. In addition, the anterior edge of the distal articular surface has a higher BV/TV, which extends up anteriorly through the epiphysis. This is in contrast to *Homo*, where BV/TV maps show a more central concentration of trabecular bone. In *Homo*, the cortex is thickest on the medial edge of the articular surface, adjacent to the medial malleolus. In several (but not all) individuals in the study sample (see Supporting Information), this medial region also has a high BV/TV. Although direct comparison between results from different subregions is complex, some of these findings are supported by the results of Su (2011). Fewer significant differences in BV/TV and cortical thickness are found across the *Homo* tibia compared to *Pan*, and *Pan* has generally higher BV/TV anteriorly and posteriorly. This is not the case for cortical thickness, where both *Homo* and *Pan* have thicker bone on the antero- and postero-medial regions, and in *Pan*, the posterocentral region of the articular surface (Su, 2011). Perhaps also relevant to the degree of flexion at the ankle, there is a region of high BV/TV and cortical thickness posterocentrally on the distal articular surface in *Pan*, with the region of high BV/TV extending into the bone. This could indicate increased loading during

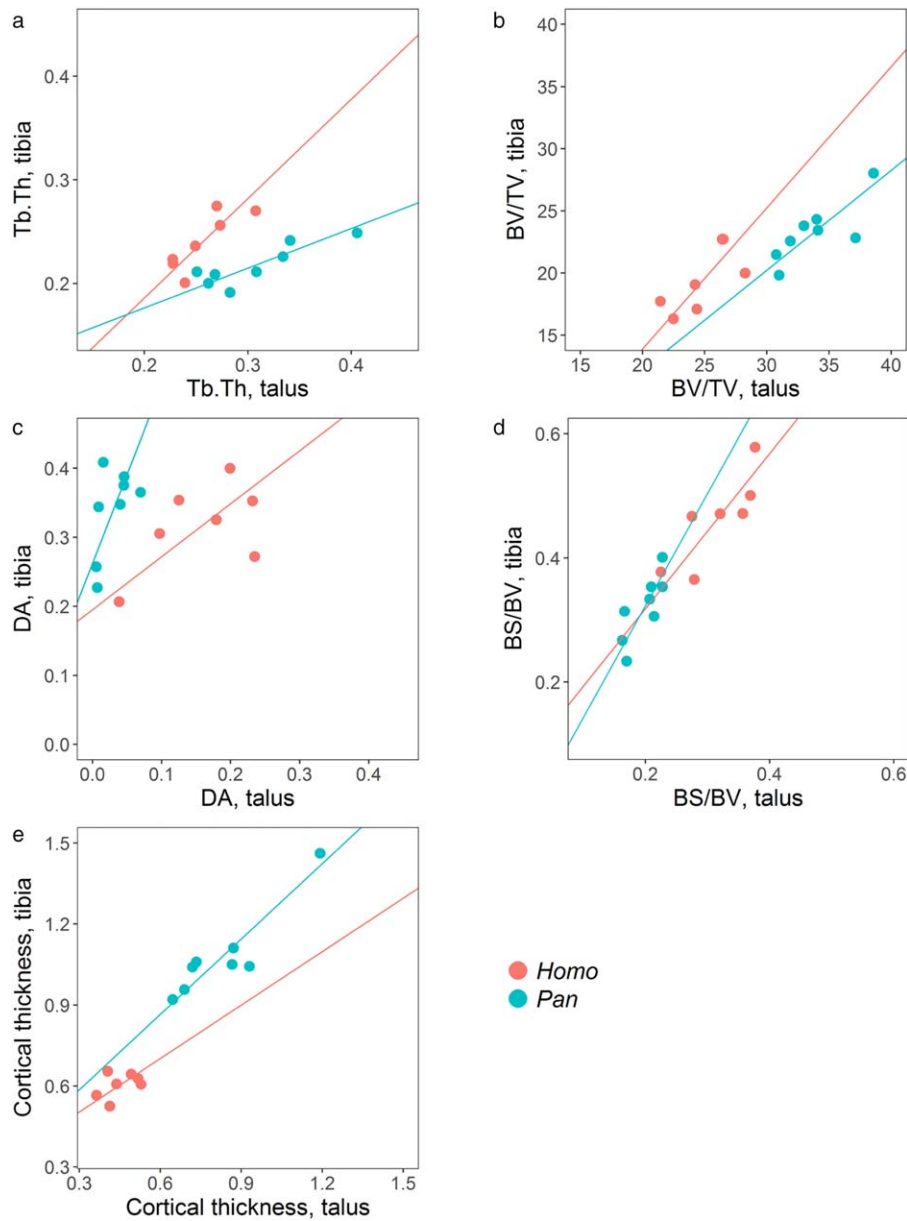


FIGURE 6 Comparison of trabecular and cortical structure between the talus and tibia in *Pan* (blue) and *Homo* (red). The log₁₀ RMA regression lines are shown independently for *Pan* (blue) and *Homo* (red)

plantarflexion in *Pan* compared to *Homo*, however, this is not supported by kinematic data. Previous findings in the distal tibia of *Pan* also found that the posterior region has a higher BV/TV than the central region, and thicker cortical bone was found in the postero-central region (Su, 2011; Su & Carlson, 2017).

In the absence of detailed kinematic data on joint contact areas, in particular for *Pan* (for humans see Bae, Park, Seon, & Jeon et al., 2015; Wan, de Asla, Rubash, & Li, 2006), our understanding of the differences in the loading of the trochlea in these two species is limited. Moreover, we must make assumptions about which aspects of a species' locomotor, or other, behavior contribute most to the remodeling of bone. Previous studies in humans have identified areas of contact and distribution of pressure on the talus using a finite element simulation of the human foot during walking (Bae et al., 2015) and on both the

talar trochlear and distal articular surface of the tibia under pressure using dual orthogonal fluoroscopy (Bischof et al., 2010; Caputo et al., 2009; Wan et al., 2006). During human bipedalism, ground reaction forces (GRF) peak at two phases, first after heelstrike and before mid-stance, and second at toe off (Alexander, 2004; Bae et al., 2015;), with contact pressure and strain increasing throughout the stride, peaking at toe off (Bae et al., 2015). After heelstrike, during the first peak in GRF, there is contact between the cartilage of the talus and tibia on the latero-central trochlea (Bae et al., 2015; Wan et al., 2006). During stride, the area of contact moves anteriorly (Bae et al., 2015; Wan et al., 2006) and the point of highest pressure moves anterocentrally until toe off, when both the contact area and point of highest pressure are located on the anterior of the trochlea, just lateral to the midline (Bae et al., 2015). At the distal tibia, contact is located anteroposteriorly at

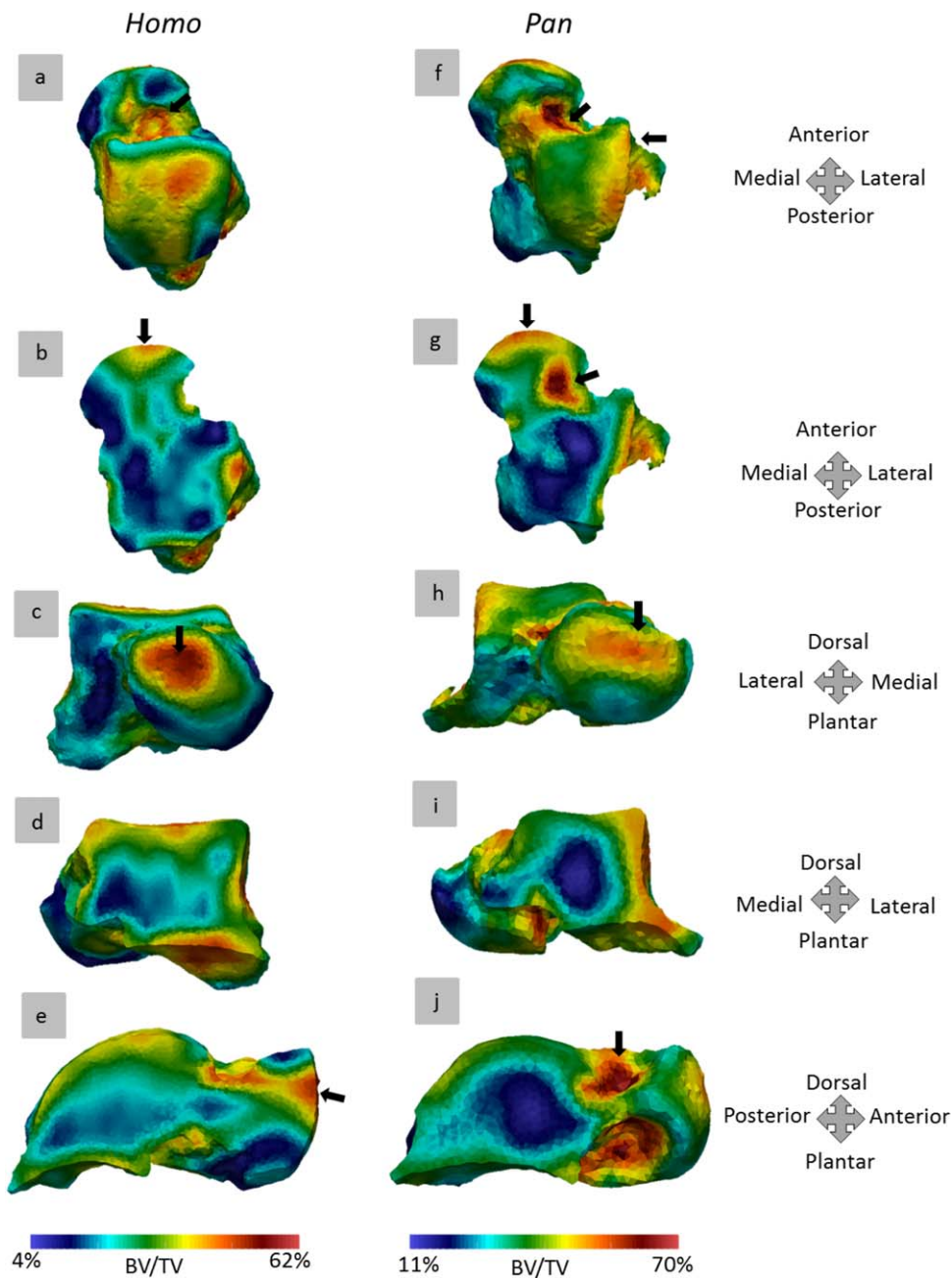


FIGURE 7 Morphometric maps of BV/TV in the talus in one individual of *Homo* (a–e) and *Pan* (f–j) in (from top to bottom) dorsal view, midtransverse plane, anterior view, coronal plane (in the center of the trochlea), and sagittal plane (in the center of the trochlea). Each specimen is scaled to its own data range, as shown in the scale bars. Black arrows indicate regions described in the text

heel strike, moving anteriorly across the mediolateral extent of the articular surface at midstance, and at heel strike in the anterolateral half of the distal articular surface of the tibia (Wan et al., 2006). Although some of the human sample in this study have a region of high BV/TV on the anterior talus, just lateral to the midline, near the location of highest pressure (Bae et al., 2015), this is not always the region of highest BV/TV, and does vary within the sample. There is also no direct correspondence between regions of contact and areas with thicker cortices. There are several potential explanations for why the trabecular and cortical bone structure of the talar trochlea does not, as expected, reflect differences in dorsiflexion at the ankle. First,

experimental measures of cartilage contact and pressure may not necessarily correspond to the regions experiencing the greatest forces during life. Second, modern humans differ greatly in their gait. For example, there is inter-individual variation in the presence of a midtarsal break, and intra-individual variation between strides (Bates et al., 2013; DeSilva et al., 2015). There is also variability in foot strike patterns, with individuals making initial contact with the fore-foot, midfoot or heel, that could also contribute to variability in loading of the trochlea (e.g., during running: Hatala, Dingwall, Wunderlich, & Richmond, 2013; Lieberman et al., 2010). Third, differences in the external morphology of the talus may accommodate the different distribution of

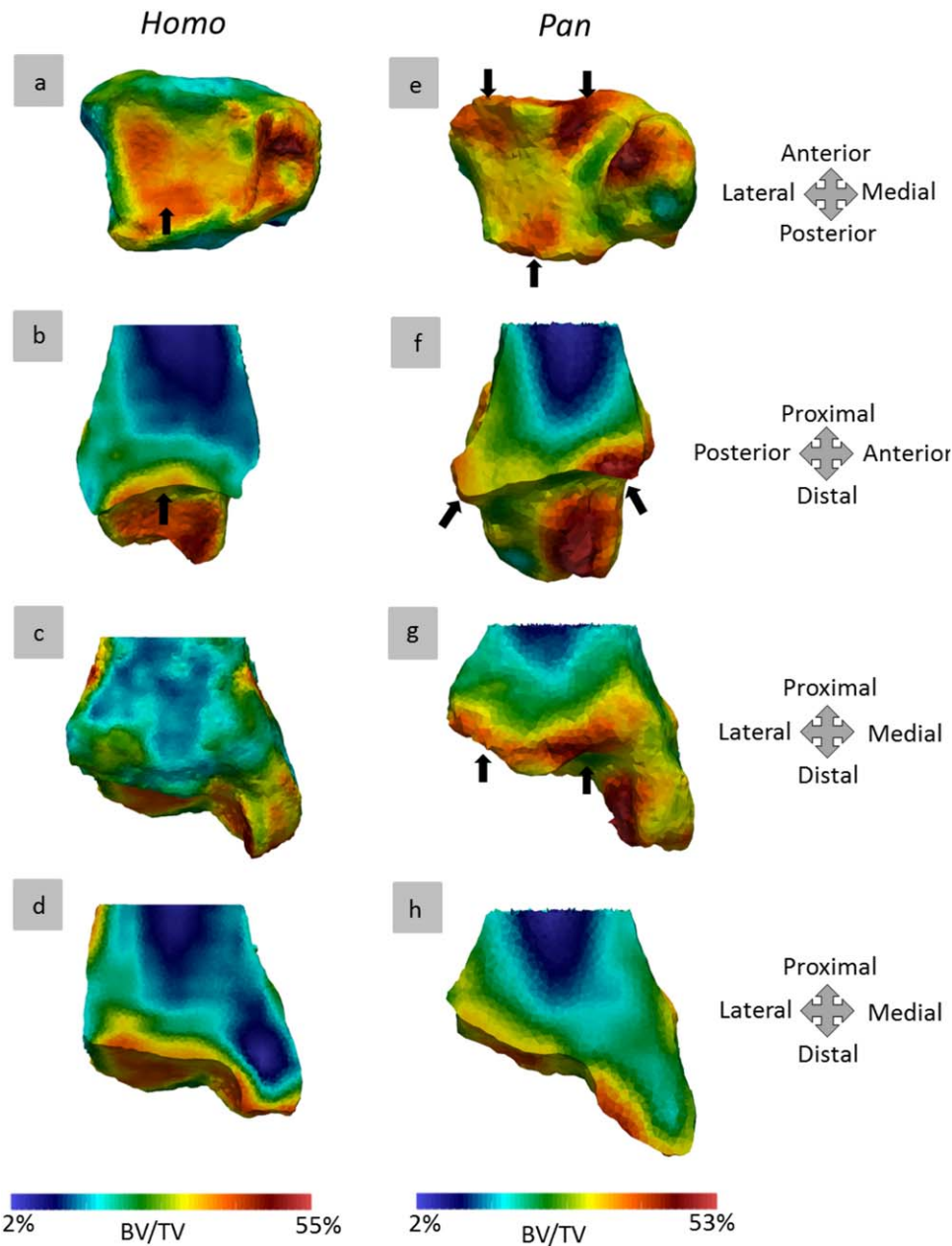


FIGURE 8 Morphometric maps of BV/TV in the tibia in one individual of *Homo* (a–d) and *Pan* (e–h) in (from top to bottom) distal view, midsagittal plane of distal tibia, anterior view, and midcoronal plane of distal tibia. Each specimen is scaled to its own data range, as shown in the scale bars. Black arrows indicate regions described in the text

forces, i.e., different shaped tali absorb loads differently, thus cortical thickness and trabecular architecture do not directly reflect differences in joint position.

Due to interest in adaptations of the human skeleton to bipedal locomotion, many biomechanical analyses of *Pan* have focused on bipedal walking (e.g., O'Neill et al., 2015; Susman, 1983; Thorpe, Crompton, & Wang, 2004; Wang, Abboud, Günther, & Crompton, 2014), although several studies have investigated kinematics of knuckle-walking in bonobos (e.g., D'Août et al., 2004; Schoonaert et al., 2016; Vereecke, D'Août, De Clercq, Van Elsaker, & Aerts, 2003). Although no *in vivo* measurements of joint movement or cartilage contact are available for *Pan*, there is evidence of force transmission due

to contact between the anterior edge of the distal tibia and the neck of the talus. This can be observed when manipulating dry, associated tibia and tali, where in an extreme position of dorsiflexion the ankle joint retains congruity while there is contact between the talar neck and the anterior border of the tibia in African apes, but not in *Homo* (Latimer et al., 1987). Modern humans who regularly adopt crouched positions develop squatting faces on the talus and tibia (Boullé, 2001). The BV/TV distribution may reflect this and indicate high loads transmitted through this region. On the medial and lateral side of the talar neck and on the anteroinferior border of the tibia, *Pan* has regions of high BV/TV, which are absent in *Homo*. This may reflect habitual loading of these regions in an ankle dorsiflexed to such a degree that force

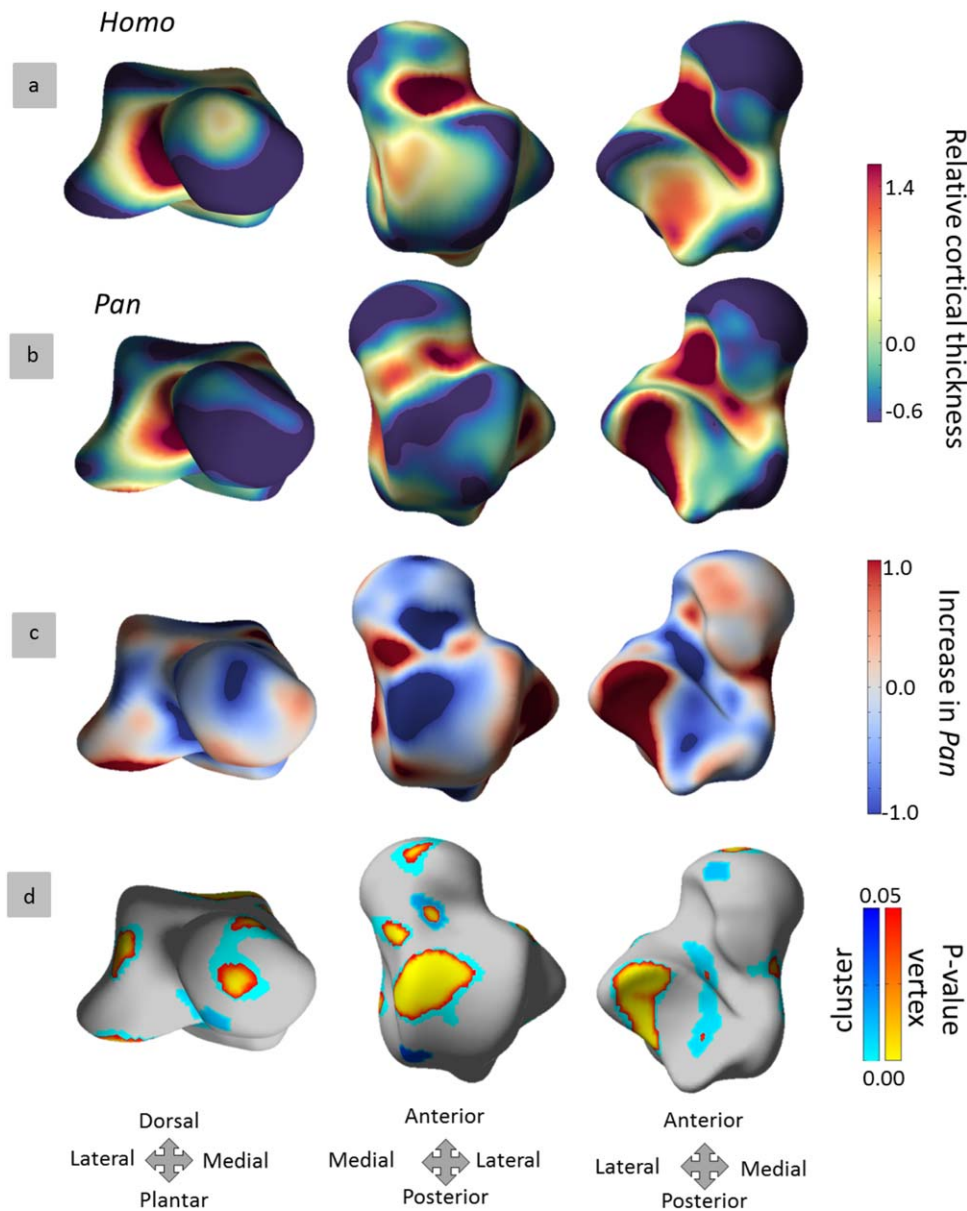


FIGURE 9 Morphometric maps of mean relative cortical thickness on the canonical talus in *Homo* (a) and *Pan* (b) in (from left to right) anterior, dorsal, and plantar views. Red indicates thick regions and blue indicates thin regions. (c) Differences between the species are shown as the difference in *Pan* compared to *Homo* with positive values (red) indicating thicker bone and negative values (blue) indicating thinner bone. (d) Regions of significant differences between the species at vertices and clusters (red-yellow) and at clusters (blue) of the surface mesh

transmission occurs between the anteroinferior edge of the distal tibia and the talar neck.

4.2.2 | Talonavicular mobility

We find a clear signal of differences in joint mobility at the talonavicular joint in the trabecular and cortical bone structure. Two features in which human bipedalism is distinct from ape quadrupedalism are, first, weight transfer from the lateral to medial side of the foot during mid-stance; and second, in having a rigid midfoot, so that the foot acts as a lever during toe off (Elftman & Manter, 1935). The medial side of the midtarsal joint (the talonavicular joint) is more mobile than the lateral side (calcaneocuboid and cuboid-MT5 joints), during stance phase the

talus rotates, along with the leg and calcaneus, creating a close packed talonavicular joint (Elftman, 1960; Scott & Winter, 1991; Siegler, Chen, & Schneck, 1988). Although investigations of midfoot mobility in *Pan* have largely focused on the midtarsal break at the lateral side (DeSilva, 2010), there is greater movement at the talonavicular joint which, during passive dorsiflexion of the foot, is characterized by rotation in the coronal plane (Thompson et al., 2014). Furthermore, there is greater inter-individual and intra-individual variability in mobility of the human lateral midfoot than was previously assumed (Bates et al., 2013; Elftman & Manter, 1935). During bipedalism, humans have greater midfoot mobility during push off, which is characterized by plantarflexion and adduction, whereas chimpanzees have higher dorsiflexion at the

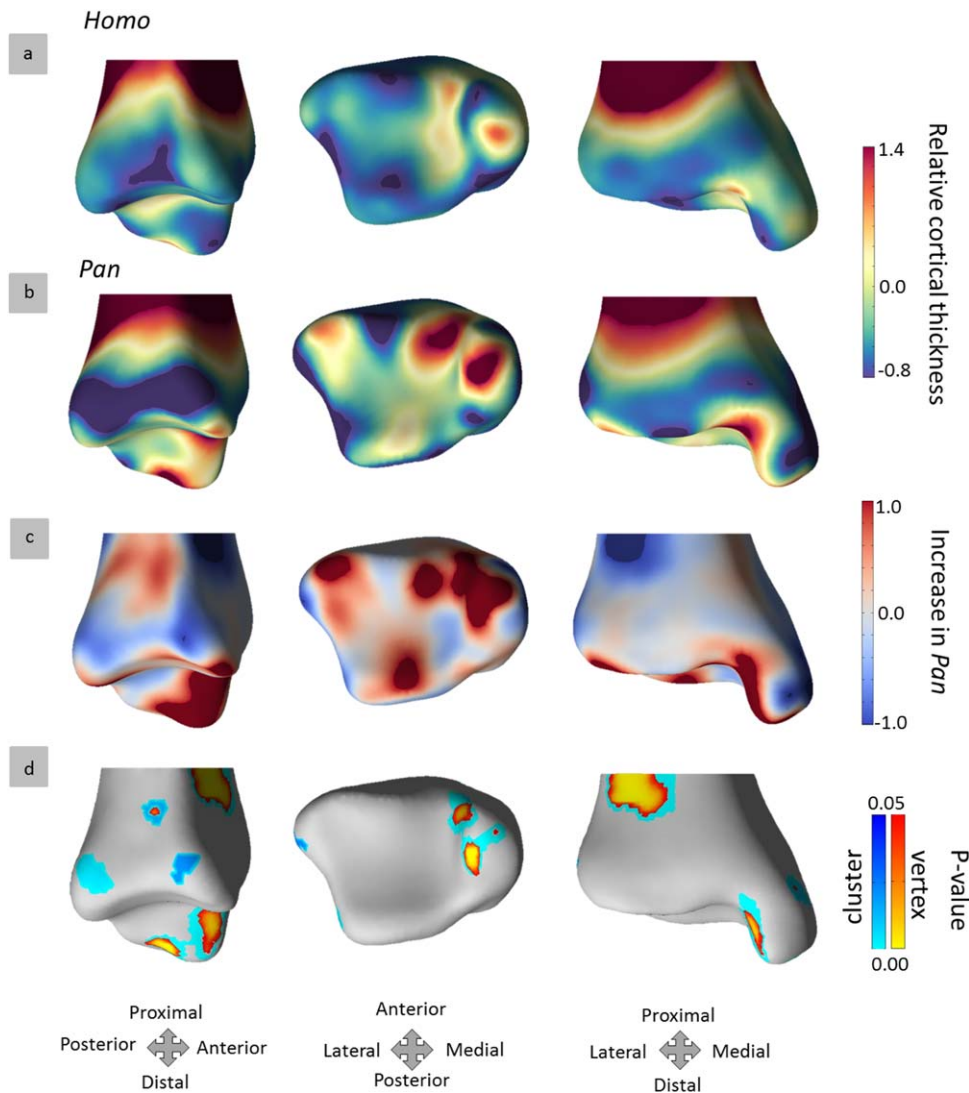


FIGURE 10 Morphometric maps of mean relative cortical thickness on the canonical tibia in (a) *Homo* and (b) *Pan* in (from left to right) lateral, distal, and anterior views. Red indicates thick regions and blue indicates thin regions. (c) Differences between the species are shown as the difference in *Pan* compared to *Homo* with positive values (red) indicating thicker bone and negative values (blue) indicating thinner bone. (d) Regions of significant differences between the species at vertices and clusters (red-yellow) and at clusters (blue) of the surface mesh

midfoot (midtarsal break) during the single limb support period (Holowka et al., 2017). Contrary to expectations, the human midfoot was found to be overall more mobile than that of chimpanzees (Holowka et al., 2017), however, precise kinematics of the talonavicular joint remain unknown.

There are clear differences between the study taxa in the trabecular bone distribution at the talar head, where *Pan* has a band of high BV/TV running mediolaterally across the talar head, and in *Homo* there is a localized point of high BV/TV. In cortical thickness, *Pan* has relatively thinner cortices at the talar head, which is significantly thinner in the central region. Previous studies have measured both trabecular bone in the medial and lateral sides of the head (DeSilva & Devlin, 2012) and trabecular bone adjacent to the neck of the talus (i.e., on the anteromedial region of the talar trochlea). When comparing the medial and lateral side of the head of the talus

in humans to other species, DeSilva and Devlin (2012) found no significant difference in DA, although the trabeculae were significantly thicker in the lateral head and significantly more connected in the medial head of humans compared to other species (DeSilva & Devlin, 2012). In the anteromedial trochlea, humans have a unique orientation of trabeculae compared to other great apes, in having trabeculae with a primarily anteroinferior orientation, i.e., parallel to the talar neck; a pattern shared with an early Pleistocene biped, KNM-ER 1464 (Su, 2011; Su & Carlson, 2017; Su et al., 2013). This distinct orientation of trabeculae in bipedal species noted by Su et al. (2013) may correspond to the trajectory of bone that we show here, travelling through the talar head into the trochlea. The trabecular and cortical distribution of the talar head reveals a clear difference in bone structure, perhaps related to differences in mid-foot mobility between the study species.

4.2.3 | Inversion

As well as dorsiflexion, inversion of the foot is characteristic of arboreal behavior in *Pan*, including vertical climbing (DeSilva, 2009). Species that engage in more arboreal locomotion have a less symmetrical trochlea surface, where the lateral trochlea ridge is higher than the medial. This asymmetry increases the difference in the radius of curvature of the medial and lateral side, thereby increasing the arcuate path of the tibia over the talus (Latimer et al., 1987), a difference that has even been identified between more arboreal western and more terrestrial eastern gorillas (Dunn, Tocheri, Orr, & Jungers, 2014). Of potential interest with regard to identifying signals of inversion, is the high BV/TV on the anterolateral lip of the trochlea of the talus that is consistent throughout the sample of *Pan*. This region also has a slightly thicker cortex in *Pan* than in *Homo*, with *Pan* having relatively thinner cortical bone than *Homo* on the anteromedial region of the trochlea. This is consistent with previous findings of high BV/TV, but not thicker cortices, on the anterolateral two thirds of the trochlea in *Pan* (Su, 2011; Su & Carlson, 2017). This may reflect increased shearing stresses associated with adoption of inverted foot postures, which are also mitigated by having a higher lateral ridge of the talus. More detailed understanding of the kinematics of climbing and knuckle-walking, along with modeling of the forces experienced by the talus, may improve interpretation of this signal.

5 | CONCLUSION

Identifying those features of internal bone structure that are directly related to joint loading is often problematic. Here, we find that average architectural variables (BV/TV, BS/BV, and cortical thickness) that relate to overall bone strength differ between *Pan* and *Homo*. These may be part of a systemic pattern unrelated to joint function, but rather due to other factors such as overall activity levels, and therefore may not be relevant for reconstructing loading of individual joints. However, the degree to which trabeculae are uniformly oriented (DA) in the talus does correspond to variation in joint loading due to different locomotor behaviors, clearly differentiating between the more stereotypical loading regime of bipedalism in *Homo* and the greater range of motion and joint loading typical of arboreal behaviors in *Pan*. In contrast to these architectural variables quantified throughout the epiphysis/bone, more precise information about locomotor behavior can be obtained from patterns of trabecular and cortical bone distribution. The trabecular and cortical bone distribution of the distal tibia and talus reflect differences in dorsiflexion at the ankle and range of motion at the talonavicular joint in humans and chimpanzees. Thus, the distribution of both trabecular and cortical bone in the talus and distal tibia holds potential for interpreting loading regimes and reconstructing loaded joint positions in fossil specimens.

ACKNOWLEDGMENTS

This research was supported by The Max Planck Society (ZJT, TLK, MMS, and JJH) and the European Research Council Starting Grant #336301 (TLK and MMS). We thank Christophe Boesch (Max Planck

Institute for Evolutionary Anthropology) and Birgit Grosskopf (University of Göttingen) for access to specimens in their care. For assistance with CT scanning, we thank David Plotzki, Heiko Temming, and Patrick Schönfeld. Helpful discussions with Nicholas Stephens and comments from two anonymous reviewers greatly improved this manuscript.

REFERENCES

- Abel, R., & Macho, G. A. (2011). Ontogenetic changes in the internal and external morphology of the ilium in modern humans. *Journal of Anatomy*, 218, 324–335.
- Ahrens, J., Geveci, B., & Law, C. (2005). ParaView: An end-user tool for large data visualization. In C. D. Hansen & C. R. Johnson (Eds.), *Visualization handbook* (pp. 717–731). Burlington, MA: Butterworth-Heinemann.
- Alexander, R. M. (2004). Bipedal animals, and their differences from humans. *Journal of Anatomy*, 204, 321–330.
- Athavale, S. A., Joshi, S. D., & Joshi, S. S. (2008). Internal architecture of the talus. *Foot & Ankle International*, 29, 82–86.
- Augat, P., & Schorlemmer, S. (2006). The role of cortical bone and its microstructure in bone strength. *Age and Ageing*, 35, 27–31.
- Bae, J. Y., Park, K. S., Seon, J. K., & Jeon, I. (2015). Analysis of the effects of normal walking on ankle joint contact characteristics after acute inversion ankle sprain. *Annals of Biomedical Engineering*, 43, 3015–3024.
- Barak, M. M., Lieberman, D. E., & Hublin, J.-J. (2011). A Wolff in sheep's clothing: Trabecular bone adaptation in response to changes in joint loading orientation. *Bone*, 49, 1141–1151.
- Barak, M. M., Lieberman, D. E., Raichlen, D., Pontzer, H., Warrener, A. G., & Hublin, J.-J. (2013). Trabecular evidence for a human-like gait in *Australopithecus africanus*. *PLoS ONE*, 8, e77687.
- Bates, K. T., Collins, D., Savage, R., McClymont, J., Webster, E., Pataky, T. C., ... Crompton, R. H. (2013). The evolution of compliance in the human lateral mid-foot. *Proceedings of the Royal Society B: Biological Sciences*, 280, 20131818.
- Beck, R. J., Andriacchi, T. P., Kuo, K. N., Fermier, R. W., & Galante, J. O. (1981). Changes in the gait patterns of growing children. *Journal of Bone and Joint Surgery*, 63A, 1452–1457.
- Behringer, V., Deschner, T., Deimel, C., Stevens, J. M. G., & Hohmann, G. (2014a). Age-related changes in urinary testosterone levels suggest differences in puberty onset and divergent life history strategies in bonobos and chimpanzees. *Hormones and Behavior*, 66, 525–533.
- Behringer, V., Deschner, T., Murtagh, R., Stevens, J. M. G., & Hohmann, G. (2014b). Age-related changes in thyroid hormone levels of bonobos and chimpanzees indicate heterochrony in development. *Journal of Human Evolution*, 66, 83–88.
- Bertram, J. E. A., & Swartz, S. M. (1991). The 'law of bone transformation': A case of crying Wolff? *Biological Reviews*, 66, 245–273.
- Biewener, A. A. (1990). Biomechanics of mammalian terrestrial locomotion. *Science*, 250, 1097–1103.
- Bischof, J. E., Spritzer, C. E., Caputo, A. M., Easley, M. E., DeOrto, J. K., Nunley, J. A., & DeFrate, L. E. (2010). In vivo cartilage contact strains in patients with lateral ankle instability. *Journal of Biomechanics*, 43, 2561–2566.
- Boulle, E.-L. (2001). Evolution of two human skeletal markers of the squatting position: A diachronic study from antiquity to the modern age. *American Journal of Physical Anthropology*, 115, 50–56.
- Caputo, A. M., Lee, J. Y., Spritzer, C. E., Easley, M. E., DeOrto, J. K., Nunley, J. A., & DeFrate, L. E. (2009). In vivo kinematics of the tibiotalar

- joint after lateral ankle instability. *The American Journal of Sports Medicine*, 37, 2241–2248.
- Carlson, K. J., Chirchir, H., & Patel, B. A. (2016). Subchondral properties of the hominoid distal tibia: An indicator of loading during habitually dorsiflexed ankle postures. *American Journal of Physical Anthropology*, 159, 109.
- Carlson, K. J., Jashashvili, T., Houghton, K., Westaway, M. C., & Patel, B. A. (2013). Joint loads in marsupial ankles reflect habitual bipedalism versus quadrupedalism. *PLoS ONE*, 8, e58811.
- Carlson, K. J., & Judex, S. (2007). Increased non-linear locomotion alters diaphyseal bone shape. *Journal of Experimental Biology*, 210, 3117–3125.
- Carlson, K. J., Lublinsky, S., & Judex, S. (2008). Do different locomotor modes during growth modulate trabecular architecture in the murine hind limb? *Integrative and Comparative Biology*, 48, 385–393.
- Chirchir, H., Kivell, T. L., Ruff, C. B., Hublin, J.-J., Carlson, K. J., Zipfel, B., & Richmond, B. G. (2015). Recent origin of low trabecular bone density in modern humans. *Proceedings of the National Academy of Sciences of the United States of America*, 112, 366–371.
- Chirchir, H., Ruff, C. B., Junno, J.-A., & Potts, R. (2017). Low trabecular bone density in recent sedentary modern humans. *American Journal of Physical Anthropology*, 162, 550–560.
- Clarke, R. J., & Tobias, P. V. (1995). Sterkfontein member 2 foot bones of the oldest South African hominid. *Science*, 269, 521–524.
- Cresswell, E. N., Goff, M. G., Nguyen, T. M., Lee, W. X., & Hernandez, C. J. (2015). Spatial relationships between bone formation and mechanical stress within cancellous bone. *Journal of Biomechanics*, 49, 222–228.
- Crompton, R. H. (2015). The hominins: A very conservative tribe? Last common ancestors, plasticity and ecomorphology in Hominidae. Or, what's in a name? *Journal of Anatomy*, 228, 686–699.
- D'Août, K., Vereecke, E., Schoonaert, K., De Clercq, D., Van Elsacker, L., & Aerts, P. (2004). Locomotion in bonobos (*Pan paniscus*): Differences and similarities between bipedal and quadrupedal terrestrial walking, and a comparison with other locomotor modes. *Journal of Anatomy*, 204, 353–361.
- Day, M. H., & Wood, B. A. (1968). Functional affinities of the Olduvai Hominid 8 talus. *Man*, 3, 440–455.
- DeSilva, J. M. (2009). Functional morphology of the ankle and the likelihood of climbing in early hominins. *Proceedings of the National Academy of Sciences of the United States of America*, 106, 6567–6572.
- DeSilva, J. M. (2010). Revisiting the “midtarsal break”. *American Journal of Physical Anthropology*, 141, 245–258.
- DeSilva, J. M., Bonne-Annee, R., Swanson, Z., Gill, C. M., Sobel, M., Uy, J., & Gill, S. V. (2015). Midtarsal break variation in modern humans: Functional causes, skeletal correlates, and paleontological implications. *American Journal of Physical Anthropology*, 156, 543–552.
- DeSilva, J. M., & Devlin, M. J. (2012). A comparative study of the trabecular bony architecture of the talus in humans, non-human primates, and *Australopithecus*. *Journal of Human Evolution*, 63, 536–551.
- DeSilva, J. M., Holt, K. G., Churchill, S. E., Carlson, K. J., Walker, C. S., Zipfel, B., & Berger, L. R. (2013). The lower limb and mechanics of walking in *Australopithecus sediba*. *Science*, 340, 1232999.
- DeSilva, J. M., & Throckmorton, Z. J. (2010). Lucy's flat feet: The relationship between the ankle and rearfoot arching in early hominins. *PLoS ONE*, 5, e14432.
- Doran, D. M. (1992). The ontogeny of chimpanzee and pygmy chimpanzee locomotor behavior: A case study of paedomorphism and its behavioral correlates. *Journal of Human Evolution*, 23, 139–157.
- Doube, M., Kłosowski, M. M., Arganda-Carreras, I., Cordelières, F. P., Dougherty, R. P., Jackson, J. S., ... Shefelbine, S. J. (2010). BoneJ: Free and extensible bone image analysis in ImageJ. *Bone*, 47, 1076–1079.
- Doube, M., Kłosowski, M. M., Wiktorowicz-Conroy, A. M., Hutchinson, J. R., & Shefelbine, S. J. (2011). Trabecular bone scales allometrically in mammals and birds. *Proceedings of the Royal Society B: Biological Sciences*, 278, 3067–3073.
- Dunn, R. H., Tocheri, M. W., Orr, C. M., & Jungers, W. L. (2014). Ecological divergence and talar morphology in gorillas. *American Journal of Physical Anthropology*, 153, 526–541.
- Ebraheim, N. A., Sabry, F. F., & Nadim, Y. (1999). Internal architecture of the talus: Implication for talar fracture. *Foot & Ankle International*, 20, 794–796.
- Ehrlich, P. J., & Lanyon, L. E. (2002). Mechanical strain and bone cell function: A review. *Osteoporosis International*, 13, 688–700.
- Eltman, H. (1960). The transverse tarsal joint and its control. *Clinical Orthopaedics*, 16, 41–46.
- Eltman, H., & Manter, J. (1935). Chimpanzee and human feet in bipedal walking. *American Journal of Physical Anthropology*, 20, 69–79.
- Friston, K. J., Holmes, A. P., Worsley, K. J., Poline, J.-P., Frith, C. D., & Frackowiak, R. S. J. (1995). Statistical parametric maps in functional imaging: A general linear approach. *Human Brain Mapping*, 2, 189–210.
- Frost, H. M. (1987). Bone “mass” and the “mechanostat”: A proposal. *The Anatomical Record*, 219, 1–9.
- Gee, A. H., & Treece, G. M. (2014). Systematic misregistration and the statistical analysis of surface data. *Medical Image Analysis*, 18, 385–393.
- Gee, A. H., Treece, G. M., Tonkin, C. J., Black, D. M., & Poole, K. E. S. (2015). Association between femur size and a focal defect of the superior femoral neck. *Bone*, 81, 60–66.
- Gosman, J. H., & Ketcham, R. A. (2009). Patterns in ontogeny of human trabecular bone from SunWatch Village in the Prehistoric Ohio Valley: General features of microarchitectural change. *American Journal of Physical Anthropology*, 138, 318–332.
- Green, R. E., Krause, J., Briggs, A. W., Maricic, T., Stenzel, U., Kircher, M., ... Pääbo, S. (2010). A draft sequence of the Neandertal genome. *Science*, 328, 710–722.
- Griffin, N. L., D'Août, K., Ryan, T. M., Richmond, B. G., Ketcham, R. A., & Postnov, A. (2010). Comparative forefoot trabecular bone architecture in extant hominids. *Journal of Human Evolution*, 59, 202–213.
- Griffin, N. L., Miller, C. E., Schmitt, D., & D'Août, K. (2015). Understanding the evolution of the windlass mechanism of the human foot from comparative anatomy: Insights, obstacles, and future directions. *American Journal of Physical Anthropology*, 156, 1–10.
- Gross, T., Kivell, T. L., Skinner, M. M., Nguyen, N. H., & Pahr, D. H. (2014). A CT-image-based framework for the holistic analysis of cortical and trabecular bone morphology. *Palaeontologia Electronica*, 17, 33A.
- Haile-Selassie, Y., Saylor, B. Z., Deino, A., Levin, N. E., Alene, M., & Latimer, B. M. (2012). A new hominin foot from Ethiopia shows multiple Pliocene bipedal adaptations. *Nature*, 483, 565–570.
- Harcourt-Smith, W. E. H., & Aiello, L. C. (2004). Fossils, feet and the evolution of human bipedal locomotion. *Journal of Anatomy*, 204, 403–416.
- Harcourt-Smith, W. E. H., Throckmorton, Z., Congdon, K. A., Zipfel, B., Deane, A. S., Drapeau, M. S. M., ... DeSilva, J. M. (2015). The foot of *Homo naledi*. *Nature Communications*, 6, 8432.
- Hatala, K. G., Dingwall, H. L., Wunderlich, R. E., & Richmond, B. G. (2013). Variation in foot strike patterns during running among habitually barefoot populations. *PLoS ONE*, 8, e52548.

- Havill, L. M., Allen, M. R., Bredbenner, T. L., Burr, D. B., Nicoletta, D. P., Turner, C. H., ... Mahaney, M. C. (2010). Heritability of lumbar trabecular bone mechanical properties in baboons. *Bone*, *46*, 835–840.
- Hérbert, D., Lebrun, R., & Marivaux, L. (2012). Comparative three-dimensional structure of the trabecular bone in the talus of primates and its relationship to ankle joint loads generated during locomotion. *The Anatomical Record*, *295*, 2069–2088.
- Holowka, N. B., O'Neill, M. C., Thompson, N. E., & Demes, B. (2017). Chimpanzee and human midfoot motion during bipedal walking and the evolution of the longitudinal arch of the foot. *Journal of Human Evolution*, *104*, 23–31.
- Hvid, I., Rasmussen, O., Jensen, N. C., & Nielsen, S. (1985). Trabecular bone strength profiles at the ankle joint. *Clinical Orthopaedics and Related Research*, *199*, 306–312.
- Ker, R. F., Bennett, M. B., Bibby, S. R., Kester, R. C., & Alexander, R. M. (1987). The spring in the arch of the human foot. *Nature*, *325*, 147–149.
- Ketcham, R. A., & Ryan, T. M. (2004). Quantification and visualization of anisotropy in trabecular bone. *Journal of Microscopy*, *213*, 158–171.
- Kivell, T. L. (2016). A review of trabecular bone functional adaptation: What have we learned from trabecular analyses in extant hominoids and what can we apply to fossils? *Journal of Anatomy*, *228*, 569–594.
- Kivell, T. L., Skinner, M. M., Lazenby, R., & Hublin, J.-J. (2011). Methodological considerations for analyzing trabecular architecture: An example from the primate hand. *Journal of Anatomy*, *218*, 209–225.
- Kraft, T. S., Venkataraman, V. V., & Dominy, N. J. (2014). A natural history of human tree climbing. *Journal of Human Evolution*, *71*, 105–118.
- Kuo, S., DeSilva, J. M., Devlin, M. J., McDonald, G., & Morgan, E. F. (2013). The effect of the Achilles tendon on trabecular structure in the primate calcaneus. *The Anatomical Record*, *296*, 1509–1517.
- Lanyon, L. E. (1974). Experimental support for the trajectorial theory of bone structure. *The Journal of Bone and Joint Surgery*, *56*, 160–166.
- Latimer, B., Ohman, J. C., & Lovejoy, C. O. (1987). Talocrural joint in African hominoids: Implications for *Australopithecus afarensis*. *American Journal of Physical Anthropology*, *74*, 155–175.
- Lazenby, R. A., Skinner, M. M., Kivell, T. L., & Hublin, J.-J. (2011). Scaling VOI size in 3D μ CT studies of trabecular bone: A test of the oversampling hypothesis. *American Journal of Physical Anthropology*, *144*, 196–203.
- Lewis, O. J. (1980a). The joints of the evolving foot. Part I. The ankle joint. *Journal of Anatomy*, *130*, 527–543.
- Lewis, O. J. (1980b). The joints of the evolving foot. Part II. The intrinsic joints. *Journal of Anatomy*, *130*, 833–857.
- Lewis, O. J. (1980c). The joints of the evolving foot. Part III. The fossil evidence. *Journal of Anatomy*, *131*, 275–298.
- Lieberman, D. E. (1996). How and why humans grow thin skulls: Experimental evidence for systemic cortical robusticity. *American Journal of Physical Anthropology*, *101*, 217–236.
- Lieberman, D. E., Venkadesan, M., Werbel, W. A., Daoud, A. I., D'Andrea, S., Davis, I. S., ... Pitsiladis, Y. (2010). Foot strike patterns and collision forces in habitually barefoot versus shod runners. *Nature*, *463*, 531–535.
- Lisowski, F. P., Albrecht, G. H., & Oxnard, C. E. (1974). The form of the talus in some higher primates: A multivariate study. *American Journal of Physical Anthropology*, *41*, 191–216.
- Lisowski, F. P., Albrecht, G. H., & Oxnard, C. E. (1976). African fossil tali: Further multivariate morphometric studies. *American Journal of Physical Anthropology*, *45*, 5–18.
- Lovejoy, C. O., McCollum, M. A., Reno, P. L., & Rosenman, B. A. (2003). Developmental biology and human evolution. *Annual Review of Anthropology*, *32*, 85–109.
- MacLachy, L., & Müller, R. (2002). A comparison of the femoral head and neck trabecular architecture of Galago and Perodicticus using micro-computed tomography (μ CT). *Journal of Human Evolution*, *43*, 89–105.
- Maga, M., Kappelman, J., Ryan, T. M., & Ketcham, R. A. (2006). Preliminary observations on the calcaneal trabecular microarchitecture of extant large-bodied hominoids. *American Journal of Physical Anthropology*, *129*, 410–417.
- Maquer, G., Musy, S. N., Wandel, J., Gross, T., & Zysset, P. K. (2015). Bone volume fraction and fabric anisotropy are better determinants of trabecular bone stiffness than other morphological variables. *Journal of Bone and Mineral Research*, *30*, 1000–1008.
- Mazurier, A., Nakatsukasa, M., & Macchiarelli, R. (2010). The inner structural variation of the primate tibial plateau characterized by high-resolution microtomography. Implications for the reconstruction of fossil locomotor behaviours. *Comptes Rendus Palevol*, *9*, 349–359.
- Morgan, E. F., & Keaveny, T. M. (2001). Dependence of yield strain of human trabecular bone on anatomic site. *Journal of Biomechanics*, *34*, 569–577.
- Morris, J. M. (1977). Biomechanics of the foot and ankle. *Clinical Orthopaedics and Related Research*, *122*, 10–17.
- Nowakowski, A. M., Deyhle, H., Zander, S., Leumann, A., & Müller-Gerbl, M. (2013). Micro CT analysis of the subarticular bone structure in the area of the talar trochlea. *Surgical and Radiologic Anatomy*, *35*, 283–293.
- Ogdaard, A. (1997). Three-dimensional methods for quantification of cancellous bone architecture. *Bone*, *20*, 315–328.
- O'Neill, M. C., Lee, L.-F., Demes, B., Thompson, N. E., Larson, S. G., Stern, J. T., Jr., & Umberger, B. R. (2015). Three-dimensional kinematics of the pelvis and hind limbs in chimpanzee (*Pan troglodytes*) and human bipedal walking. *Journal of Human Evolution*, *86*, 32–42.
- Oxnard, C. E., & Lisowski, F. P. (1980). Functional articulation of some hominoid foot bones: Implications for the Olduvai (Hominid 8) foot. *American Journal of Physical Anthropology*, *52*, 107–117.
- Pal, G. P., & Routal, R. V. (1998). Architecture of the cancellous bone of the human talus. *The Anatomical Record*, *252*, 185–193.
- Patel, B. A., & Carlson, K. J. (2007). Bone density spatial patterns in the distal radius reflect habitual hand postures adopted by quadrupedal primates. *Journal of Human Evolution*, *52*, 130–141.
- Paternoster, L., Lorentzon, M., Lehtimäki, T., Eriksson, J., Kähönen, M., Raitakari, O., ... Ohlsson, C. (2013). Genetic determinants of trabecular and cortical volumetric bone mineral densities and bone microstructure. *PLoS Genetics*, *9*, e1003247.
- Pearson, O. M., & Lieberman, D. E. (2004). The aging of Wolff's 'law': Ontogeny and responses to mechanical loading in cortical bone. *Yearbook of Physical Anthropology*, *47*, 63–99.
- Pettersson, U., Nilsson, M., Sundh, V., Mellström, D., & Lorentzon, M. (2010). Physical activity is the strongest predictor of calcaneal peak bone mass in young Swedish men. *Osteoporosis International*, *21*, 447–455.
- Polk, J. D., Blumenfeld, J., & Ahluwalia, D. (2008). Knee posture predicted from subchondral apparent density in the distal femur: An experimental validation. *The Anatomical Record*, *291*, 293–302.
- Polk, J. D., Williams, S. A., Peterson, J. V., Roseman, C. C., & Godfrey, L. R. (2010). Subchondral bone apparent density and locomotor behavior in extant primates and subfossil lemurs Hadropithecus and Pachylemur. *International Journal of Primatology*, *31*, 275–299.

- Pontzer, H., Lieberman, D. E., Momin, E., Devlin, M. J., Polk, J. D., Hallgrímsson, B., & Cooper, D. M. L. (2006). Trabecular bone in the bird knee responds with high sensitivity to changes in load orientation. *The Journal of Experimental Biology*, 209, 57–65.
- Pontzer, H., Raichlen, D. A., & Rodman, P. S. (2014). Bipedal and quadrupedal locomotion in chimpanzees. *Journal of Human Evolution*, 66, 64–82.
- Pontzer, H., Raichlen, D. A., & Sockol, M. D. (2009). The metabolic cost of walking in humans, chimpanzees, and early hominins. *Journal of Human Evolution*, 56, 43–54.
- Prang, T. C. (2015). Rearfoot posture of *Australopithecus sediba* and the evolution of the hominin longitudinal arch. *Scientific Reports*, 5, 17677.
- Prang, T. C. (2016). The subtalar joint complex of *Australopithecus sediba*. *Journal of Human Evolution*, 90, 105–119.
- R Core Team. (2016). *R: A language and environment for statistical computing*. Vienna, Austria: R Foundation for Statistical Computing.
- Raichlen, D. A., Gordon, A. D., Foster, A. D., Webber, J. T., Sukhdeo, S. M., Scott, R. S., ... Ryan, T. M. (2015). An ontogenetic framework linking locomotion and trabecular bone architecture with applications for reconstructing hominin life history. *Journal of Human Evolution*, 81, 1–12.
- Robling, A. G., Hinant, F. M., Burr, D. B., & Turner, C. H. (2002). Improved bone structure and strength after long-term mechanical loading is greatest if loading is separated into short bouts. *Journal of Bone and Mineral Research*, 17, 1545–1554.
- Rubin, C. T., & Lanyon, L. E. (1985). Regulation of bone mass by mechanical strain magnitude. *Calcified Tissue International*, 37, 411–417.
- Ruff, C. B. (2005). Mechanical determinants of bone form: Insights from skeletal remains. *Journal of Musculoskeletal Neuronal Interactions*, 5, 202–212.
- Ruff, C., Holt, B., & Trinkaus, E. (2006). Who's afraid of the big bad Wolff? "Wolff's law" and bone functional adaptation. *American Journal of Physical Anthropology*, 129, 484–498.
- Ruff, C. B., & Runestad, J. A. (1992). Primate limb bone structural adaptations. *Annual Review of Anthropology*, 21, 407–433.
- Ruff, C. B., Trinkaus, E., Walker, A., & Larsen, C. S. (1993). Postcranial robusticity in Homo, I: Temporal trends and mechanical interpretation. *American Journal of Physical Anthropology*, 91, 21–53.
- Ryan, T. M., & Ketcham, R. A. (2002a). The three-dimensional structure of trabecular bone in the femoral head of strepsirrhine primates. *Journal of Human Evolution*, 43, 1–26.
- Ryan, T. M., & Ketcham, R. A. (2002b). Femoral head trabecular bone structure in two omomyid primates. *Journal of Human Evolution*, 43, 241–263.
- Ryan, T. M., & Krovitz, G. E. (2006). Trabecular bone ontogeny in the human proximal femur. *Journal of Human Evolution*, 51, 591–602.
- Ryan, T. M., & Shaw, C. N. (2015). Gracility of the modern *Homo sapiens* skeleton is the result of decreased biomechanical loading. *Proceedings of the National Academy of Sciences of the United States of America*, 112, 372–377.
- Ryan, T. M., van Rietbergen, B., & Krovitz, G. (2007). Mechanical adaptation of the trabecular bone in the growing human femur and humerus. *American Journal of Physical Anthropology*, 44, 203.
- Sarringhaus, L. A., MacLatchy, L. M., & Mitani, J. C. (2014). Locomotor and postural development of wild chimpanzees. *Journal of Human Evolution*, 66, 29–38.
- Scherf, H., & Tilgner, R. (2009). A new high-resolution computed tomography (CT) segmentation method for trabecular bone architectural analysis. *American Journal of Physical Anthropology*, 140, 39–51.
- Scherf, H., Wahl, J., Hublin, J.-J., & Harvati, K. (2015). Patterns of activity adaptation in humeral trabecular bone in Neolithic humans and present-day people. *American Journal of Physical Anthropology*, 159, 106–115.
- Schiff, A., Li, J., Inoue, N., Masuda, K., Lidtke, R., & Muehleman, C. (2007). Trabecular angle of the human talus is associated with the level of cartilage degeneration. *Journal of Musculoskeletal and Neuronal Interactions*, 7, 224–230.
- Schneider, C. A., Rasband, W. S., & Eliceiri, K. W. (2012). NIH Image to ImageJ: 25 years of image analysis. *Nature Methods*, 9, 671–675.
- Schoonaert, K., D'Août, K., Samuel, D., Talloen, W., Nauwelaerts, S., Kivell, T. L., & Aerts, P. (2016). Gait characteristics and spatio-temporal variables of climbing in bonobos (*Pan paniscus*). *American Journal of Primatology*, 78, 1165–1177.
- Schulte, F. A., Ruffoni, D., Lambers, F. M., Christen, D., Webster, D. J., Kuhn, G., & Müller, R. (2013). Local mechanical stimuli regulate bone formation and resorption in mice at the tissue level. *PLoS ONE*, 8, e62172.
- Scott, S. H., & Winter, D. A. (1991). Talocrural and talocalcaneal joint kinematics and kinetics during the stance phase of walking. *Journal of Biomechanics*, 24, 743–752.
- Siegler, S., Chen, J., & Schneck, C. D. (1988). The three-dimensional kinematics and flexibility characteristics of the human ankle and subtalar joints: Part I: Kinematics. *Journal of Biomechanical Engineering*, 110, 364–373.
- Singh, I. (1978). The architecture of cancellous bone. *Journal of Anatomy*, 127, 305–310.
- Sinha, D. N. (1985). Cancellous structure of tarsal bones. *Journal of Anatomy*, 140, 111–117.
- Skerry, T. M., & Lanyon, L. E. (1995). Interruption of disuse by short duration walking exercise does not prevent bone loss in the sheep calcaneus. *Bone*, 16, 269–274.
- Skinner, M. M., Stephens, N. B., Tsegai, Z. J., Foote, A. C., Nguyen, N. H., Gross, T., ... Kivell, T. L. (2015). Human-like hand use in *Australopithecus africanus*. *Science*, 347, 395–399.
- Smith, R. J., & Jungers, W. L. (1997). Body mass in comparative primatology. *Journal of Human Evolution*, 32, 523–559.
- Sockol, M. D., Raichlen, D. A., & Pontzer, H. (2007). Chimpanzee locomotor energetics and the origin of human bipedalism. *Proceedings of the National Academy of Sciences of the United States of America*, 104, 12265–12269.
- Sode, M., Burghardt, A. J., Nissenon, R. A., & Majumdar, S. (2008). Resolution dependence of the non-metric trabecular structure indices. *Bone*, 42, 728–736.
- Stauber, M., Rapillard, L., van Lenthe, G. H., Zysset, P., & Müller, R. (2006). Importance of individual rods and plates in the assessment of bone quality and their contribution to bone stiffness. *Journal of Bone and Mineral Research*, 21, 586–595.
- Stern, J. T., & Susman, R. L. (1983). The locomotor anatomy of *Australopithecus afarensis*. *American Journal of Physical Anthropology*, 60, 279–317.
- Su, A. (2011). *The functional morphology of subchondral and trabecular bone in the hominoid tibiotalar joint*. (Doctoral dissertation), The Graduate School, Stony Brook University: Stony Brook, NY.
- Su, A., & Carlson, K. J. (2017). Comparative analysis of trabecular bone structure and orientation in South African hominin tali. *Journal of Human Evolution*, 106, 1–18.
- Su, A., Wallace, I. J., & Nakatsukasa, M. (2013). Trabecular bone anisotropy and orientation in an Early Pleistocene hominin talus from East Turkana, Kenya. *Journal of Human Evolution*, 64, 667–677.
- Susman, R. L. (1983). Evolution of the human foot: Evidence from Pliocene hominids. *Foot & Ankle*, 3, 365–376.

- Sutherland, D. H., Olshen, R., Cooper, L., & Woo, S. L. Y. (1980). The development of mature gait. *Journal of Bone and Joint Surgery*, *62A*, 336–353.
- Takechi, H., Ito, S., Takada, T., & Nakayama, H. (1982). Trabecular architecture of the ankle joint. *Anatomia Clinica*, *4*, 227–233.
- Thompson, N. E., Holowka, N. B., O'Neill, M. C., & Larson, S. G. (2014). Brief communication: Cineradiographic analysis of the chimpanzee (*Pan troglodytes*) talonavicular and calcaneocuboid joints. *American Journal of Physical Anthropology*, *154*, 604–608.
- Thorpe, S. K. S., Crompton, R. H., & Wang, W. J. (2004). Stresses exerted in the hindlimb muscles of common chimpanzees (*Pan troglodytes*) during bipedal locomotion. *Folia Primatologica*, *75*, 253–265.
- Treece, G. M., Gee, A. H., Mayhew, P. M., & Poole, K. E. S. (2010). High resolution cortical bone thickness measurement from clinical CT data. *Medical Image Analysis*, *14*, 276–290.
- Treece, G. M., Poole, K. E. S., & Gee, A. H. (2012). Imaging the femoral cortex: Thickness, density and mass from clinical CT. *Medical Image Analysis*, *16*, 952–965.
- Tsegai, Z. J., Kivell, T. L., Gross, T., Nguyen, N. H., Pahr, D. H., Smaers, J. B., & Skinner, M. M. (2013). Trabecular bone structure correlates with hand posture and use in hominoids. *PLoS ONE*, *8*, e78781.
- Tsegai, Z. J., Skinner, M. M., Pahr, D. H., Hublin, J.-J., & Kivell, T. L. (2016). Systemic patterns of trabecular structure in *Homo* and *Pan*: Evaluating inter- and intraspecific variability across anatomical sites. *American Journal of Physical Anthropology*, *159*, 318.
- Tsegai, Z. J., Stephens, N. S., Treece, G., Skinner, M. M., Kivell, K. L., & Gee, A. (2017). Cortical bone mapping: An application to hand and foot bones in hominoids. *Comptes Rendus Palevol*, doi:10.1016/j.crvp.2016.11.001.
- Turner, A. S. (2001). Animal models of osteoporosis—Necessity and limitations. *European Cells and Materials*, *1*, 66–81.
- Venkataraman, V. V., Kraft, T. S., DeSilva, J. M., & Dominy, N. J. (2013). Phenotypic plasticity of climbing-related traits in the ankle joint of great apes and rainforest hunter-gatherers. *Human Biology*, *85*, 309–328.
- Venkataraman, V. V., Kraft, T. S., & Dominy, N. J. (2013). Tree climbing and human evolution. *Proceedings of the National Academy of Sciences of the United States of America*, *110*, 1237–1242.
- Vereecke, E., D'Août, K., De Clercq, D., Van Elsaker, L., & Aerts, P. (2003). Dynamic plantar pressure distribution during terrestrial locomotion of bonobos (*Pan paniscus*). *American Journal of Physical Anthropology*, *120*, 373–383.
- Wallace, I. J., Kwaczala, A. T., Judex, S., Demes, B., & Carlson, K. J. (2013). Physical activity engendering loads from diverse directions augments the growing skeleton. *Journal of Musculoskeletal and Neural Interactions*, *13*, 283–288.
- Wallace, I. J., Middleton, K. M., Lublinsky, S., Kelly, S. A., Judex, S., Garland, T., & Demes, B. (2010). Functional significance of genetic variation underlying limb bone diaphyseal structure. *American Journal of Physical Anthropology*, *143*, 21–30.
- Wan, L., de Asla, R. J., Rubash, H. E., & Li, G. (2006). Determination of in-vivo articular cartilage contact areas of human talocrural joint under weightbearing conditions. *Osteoarthritis and Cartilage*, *14*, 1294–1301.
- Wang, W., Abboud, R. J., Günther, M. M., & Crompton, R. H. (2014). Analysis of joint force and torque for the human and non-human ape foot during bipedal walking with implications for the evolution of the foot. *Journal of Anatomy*, *225*, 152–166.
- Whitehouse, W. J. (1974). The quantitative morphology of anisotropic trabecular bone. *Journal of Microscopy*, *101*, 153–168.
- Wickham, H. (2009). *ggplot2: Elegant graphics for data analysis*. New York: Springer-Verlag.
- Worsley, K. J., Taylor, J. E., Carbonell, F., Chung, M. K., Duerden, E., Bernhardt, B., ... Evans, A. C. (2009). SurfStat: A Matlab toolbox for the statistical analysis of univariate and multivariate surface and volumetric data using linear mixed effects models and random field theory. *NeuroImage*, *47*, S102.
- Zeininger, A., Patel, B. A., Zipfel, B., & Carlson, K. J. (2016). Trabecular architecture in the StW 352 fossil hominin calcaneus. *Journal of Human Evolution*, *97*, 145–158.
- Zeininger, A., Richmond, B. G., & Hartman, G. (2011). Metacarpal head biomechanics: A comparative backscattered electron image analysis of trabecular bone mineral density in *Pan troglodytes*, *Pongo pygmaeus*, and *Homo sapiens*. *Journal of Human Evolution*, *60*, 703–710.
- Zipfel, B., DeSilva, J. M., Kidd, R. S., Carlson, K. J., Churchill, S. E., & Berger, L. R. (2011). The foot and ankle of *Australopithecus sediba*. *Science*, *333*, 1417–1420.

SUPPORTING INFORMATION

Additional Supporting Information may be found online in the supporting information tab for this article.

How to cite this article: Tsegai ZJ, Skinner MM, Gee AH, et al. Trabecular and cortical bone structure of the talus and distal tibia in *Pan* and *Homo*. *Am J Phys Anthropol*. 2017;163:784–805. <https://doi.org/10.1002/ajpa.23249>